JAERI-Research
97-053

ANALYSIS OF THE JAERI CRITICAL HEAT FLUX DATA BASE FOR FUSION APPLICATION

August 1997

Jean BOSCARY*, Masanori ARAKI and Masato AKIBA

日本原子力研究所
Japan Atomic Energy Research Institute

本レポートは，日本原子力研究所が不定期に公刊している研究報告書です。
入手の問合わせは，日本原子力研究所研究情報部研究情報課（〒319-11 茨城県那珂郡東海村）あて，お申し越しください。なお，このほかに財団法人原子力弘済会資料センター（〒319-11 茨城県那珂郡東海村日本原子力研究所内）で複写による実費頒布をおこなっております。

This report is issued irregularly.
Inquiries about availability of the reports should be addressed to Research Information Division, Department of Intellectual Resources, Japan Atomic Energy Research Institute, Tokai-mura, Naka-gun, Ibaraki-ken, 319-11, Japan.

編集兼発行　日本原子力研究所
印　　刷　いばらき印刷㈱

JAERI-Research 97-053

Analysis of the JAERI Critical Heat Flux Data Base for Fusion Application

Jean BOSCARY*, Masanori ARAKI+ and Masato AKIBA

Department of Fusion Engineering Research
Naka Fusion Research Establishment
Japan Atomic Energy Research Institute
Naka-machi, Naka-gun, Ibaraki-ken

(Received July 11, 1997)

This report presents a complete review of the critical heat flux (CHF) experiments performed by JAERI in the thermal hydraulic conditions of fusion reactors: one-side heating, high heat flux and water-cooled. Different geometries were tested: smooth tube, externally finned swirl tube, screw tube and hypervapotron. Externally finned swirl tube and screw tubes are the most efficient and show similar performances. The effect of experimental thermal hydraulic conditions on CHF, detected by thermocouples located in the material, is analyzed. Within the range of experiments, the mass flux has a strong influence on the CHF and the pressure has a weak effect on CHF. Experimental results for smooth and externally finned swirl tubes are predicted by Inasaka et Nariai and modified correlation with a $\pm 20\%$ accuracy.

Keywords: Divertor Plate, Critical Heat Flux, Subcooled Boiling, One-side Heating, Screw Tube, Swirl Tube, Hypervapotron

---

+ Department of ITER Project

* Science and Technology Agency fellow

原研における核融合実験炉用限界熱流束データベースの解析

日本原子力研究所那珂研究所核融合工学部
Jean BOSCARY*・荒木　政則+・秋場　真人

(1997年7月11日受理)

本報告はこれまで原研において核融合実験炉を模擬した伝熱流動条件－片面加熱場、高熱流束、水冷－の下で実施された限界熱流束（ＣＨＦ）実験の結果をまとめたものである。平滑管、外部フィン付きスワール管、スクリュウ管及びハイパーベイパートロンが実験に供試された。外部フィン付きスワール管とスクリュウ管の性能は殆ど等しく、供試された冷却管の中で最も高い限界熱流束を示した。実験条件の範囲内では、冷却水の質量流量がＣＨＦに大きな影響を与え、冷却水の圧力はＣＨＦに殆ど影響を与えないことがわかった。平滑管と外部フィン付きスワール管の限界熱流束は，限界熱流束相関式であるInasaka-Nariai式によって±20%の精度で予測可能であることが明らかになった。

那珂研究所：〒311－01　茨城県那珂郡那珂町向山801－1
+ ＩＴＥＲ開発室
* 科学技術庁リサーチフェロー

Contents

目　　次

1. INTRODUCTION

For the next generation of thermonuclear fusion machine as the International Thermonuclear Experimental Reactor, ITER, some components facing to plasma will be exposed to high heat fluxes of several tens of MW/m^2. The design of divertor plates requires the development of a high performance cooling device with pressurized subcooled water flow under one-side heating conditions. Various concepts have been proposed and tested by laboratories working on the cooling of high heat flux components for fusion application (see Ref. 1 to Ref. 7). For design purpose, it is important to predict with accuracy the Critical Heat Flux (CHF) versus the thermal hydraulic conditions. This report presents a complete review and analysis of the CHF experiments performed by JAERI for different geometries: smooth tube, externally finned swirl tube, screw tube and hypervapotron. In section 2, experimental conditions are briefly reported. In sections 3 and 4, experimental results are presented and the influence of thermal hydraulic parameters on CHF is analyzed. Section 5 deals with CHF modeling. Test results of smooth and externally finned swirl tube are compared with Tong 75 correlation, which is extensively used and adapted so far to predict CHF for fusion application.

2. EXPERIMENTAL CONDITIONS

Experimental conditions, previously presented in Ref. 8, are briefly reported. Tests were carried out in an Ion Beam facility of JAERI, or Particle Beam Engineering test Facility (PBEF) presented in Fig. 1. Test sections, 400 mm long, were made of OFHC-Cu. General conditions of experiments are described in Fig. 2. The incident heat flux and the incident profile were measured with a multi-channel calorimeter. The longitudinal profile along the flow direction is almost Gaussian with a full width at half maximum of 120 mm.

Each mock-up was equipped with 5 type-K thermocouples whose outer diameter is 0.5 mm. The distance between two consecutive thermocouples was 10 mm. Each thermocouple was located 0.2 mm below the heated surface of the test section. CHF was detected by thermocouples whose trigger value was set between 500 and 550°C. CHF event was caught by the third and the fourth thermocouple located at 10 mm and at 20 mm downstream from the centre of the mock-up, respectively. Due to a rapid

1. INTRODUCTION

For the next generation of thermonuclear fusion machine as the International Thermonuclear Experimental Reactor, ITER, some components facing to plasma will be exposed to high heat fluxes of several tens of MW/m^2. The design of divertor plates requires the development of a high performance cooling device with pressurized subcooled water flow under one-side heating conditions. Various concepts have been proposed and tested by laboratories working on the cooling of high heat flux components for fusion application (see Ref. 1 to Ref. 7). For design purpose, it is important to predict with accuracy the Critical Heat Flux (CHF) versus the thermal hydraulic conditions. This report presents a complete review and analysis of the CHF experiments performed by JAERI for different geometries: smooth tube, externally finned swirl tube, screw tube and hypervapotron. In section 2, experimental conditions are briefly reported. In sections 3 and 4, experimental results are presented and the influence of thermal hydraulic parameters on CHF is analyzed. Section 5 deals with CHF modeling. Test results of smooth and externally finned swirl tube are compared with Tong 75 correlation, which is extensively used and adapted so far to predict CHF for fusion application.

2. EXPERIMENTAL CONDITIONS

Experimental conditions, previously presented in Ref. 8, are briefly reported. Tests were carried out in an Ion Beam facility of JAERI, or Particle Beam Engineering test Facility (PBEF) presented in Fig. 1. Test sections, 400 mm long, were made of OFHC-Cu. General conditions of experiments are described in Fig. 2. The incident heat flux and the incident profile were measured with a multi-channel calorimeter. The longitudinal profile along the flow direction is almost Gaussian with a full width at half maximum of 120 mm.

Each mock-up was equipped with 5 type-K thermocouples whose outer diameter is 0.5 mm. The distance between two consecutive thermocouples was 10 mm. Each thermocouple was located 0.2 mm below the heated surface of the test section. CHF was detected by thermocouples whose trigger value was set between 500 and 550°C. CHF event was caught by the third and the fourth thermocouple located at 10 mm and at 20 mm downstream from the centre of the mock-up, respectively. Due to a rapid

spread of the dry-out region, the location of CHF occurrence was considered as the position of the third thermocouple, *i.e.*, located at 10 mm from the centre of the test section. This location does not correspond exactly to the peak of the heat flux profile.

3. EXPERIMENTAL RESULTS

Four geometries were mainly tested: smooth tube, externally finned swirl tube, screw tube and hypervapotron. Characteristics are presented in Fig. 3. A total of 59 tests was performed, the distribution according to the different geometries is shown in Fig. 4. Due to operating conditions of the facility, the main investigated parameter was the mass flux, whose maximal value was limited by the pressure drop of the test section. In next figures, error bars represent a ± 15% uncertainty of the incident heat flux measurement.

3.1. Smooth tube

Experimental range was:

$$6 \leq G \leq 25 \text{ Mg.m}^{-2}.\text{s}^{-1};\ T_{in} = 30°C;\ P = 1 \text{ MPa}.$$

A smooth tube is able to withstand high incident heat fluxes: 15.3 MW/m^2 for G = 6 Mg.m^{-2}.s^{-1}, which was the minimal investigated mass flux. Fig. 5 shows that Incident CHF is an increasing function of the mass flux G, but this effect appears to be weak from 15 Mg.m^{-2}.s^{-1}.

3.2. Externally finned swirl tube

Experimental range was:

$$4 \leq G \leq 14 \text{ Mg.m}^{-2}.\text{s}^{-1};\ T_{in} = 25°C;\ P = 1.0,\ 1.5 \text{ MPa}.$$

This tube is very efficient, especially at a low mass flux: 21.8 MW/m^2 for G = 4 Mg.m^{-2}.s^{-1} and P = 1 MPa. Fig. 6 shows that Incident CHF is an increasing function of the mass flux. The effect of the pressure on the Incident CHF is slight.

3.3. Screw tube

Experimental range was:

$$2 \leq G \leq 20 \text{ Mg.m}^{-2}.\text{s}^{-1};\ T_{in} = 30°C;\ P = 1 \text{ MPa}.$$

spread of the dry-out region, the location of CHF occurrence was considered as the position of the third thermocouple, *i.e.*, located at 10 mm from the centre of the test section. This location does not correspond exactly to the peak of the heat flux profile.

3. EXPERIMENTAL RESULTS

Four geometries were mainly tested: smooth tube, externally finned swirl tube, screw tube and hypervapotron. Characteristics are presented in Fig. 3. A total of 59 tests was performed, the distribution according to the different geometries is shown in Fig. 4. Due to operating conditions of the facility, the main investigated parameter was the mass flux, whose maximal value was limited by the pressure drop of the test section. In next figures, error bars represent a ± 15% uncertainty of the incident heat flux measurement.

3.1. Smooth tube

Experimental range was:

$$6 \leq G \leq 25 \text{ Mg.m}^{-2}.\text{s}^{-1};\ T_{in} = 30°C;\ P = 1 \text{ MPa}.$$

A smooth tube is able to withstand high incident heat fluxes: 15.3 MW/m^2 for G = 6 Mg.m^{-2}.s^{-1}, which was the minimal investigated mass flux. Fig. 5 shows that Incident CHF is an increasing function of the mass flux G, but this effect appears to be weak from 15 Mg.m^{-2}.s^{-1}.

3.2. Externally finned swirl tube

Experimental range was:

$$4 \leq G \leq 14 \text{ Mg.m}^{-2}.\text{s}^{-1};\ T_{in} = 25°C;\ P = 1.0,\ 1.5 \text{ MPa}.$$

This tube is very efficient, especially at a low mass flux: 21.8 MW/m^2 for G = 4 Mg.m^{-2}.s^{-1} and P = 1 MPa. Fig. 6 shows that Incident CHF is an increasing function of the mass flux. The effect of the pressure on the Incident CHF is slight.

3.3. Screw tube

Experimental range was:

$$2 \leq G \leq 20 \text{ Mg.m}^{-2}.\text{s}^{-1};\ T_{in} = 30°C;\ P = 1 \text{ MPa}.$$

Three different configurations were studied: M7, M12 and M16 based on ISO-261 standard (see Fig. 3). The ratio between the fin height and the pitch is constant and is equal to 1.15. The best result was obtained with M7: ICHF = 41.6 MW/m^2 for G = 20 Mg.m^{-2}.s^{-1}. Fig. 8 shows that the Incident CHF is an increasing function of the mass flux for the different types of screw tubes. Fig. 8 also indicates a weak effect of the screw type on the Incident CHF, especially between G = 5 Mg.m^{-2}.s^{-1} and G = 12 Mg.m^{-2}.s^{-1}.

3.4. Hypervapotron

Experimental range was:

$$2 \leq G \leq 10 \text{ Mg.m}^{-2}.\text{s}^{-1};\ T_{in} = 30°C;\ P = 0.7,\ 1.0 \text{ MPa}.$$

This tube is able to remove high heat fluxes of about 20 - 25 MW/m^2. Fig. 7 shows that Incident CHF is an increasing function of the mass flux. It can be noticed an important step at low mass flux and P = 1 MPa: ICHF = 6.8 MW/m^2 for G = 2 Mg.m^{-2}.s^{-1} and ICHF = 19.8 MW/m^2 for G = 4 Mg.m^{-2}.s^{-1}, that is to say a 2.9 enhancement factor. This effect is much less important from G = 4 Mg.m^{-2}.s^{-1} and P = 1 MPa: ICHF = 19.8 MW/m^2 for G = 4 Mg.m^{-2}.s^{-1} and ICHF = 25.3 MW/m^2 for G = 10 Mg.m^{-2}.s^{-1}. This effect may come from an evolution of the heat transfer process at the wall. At low mass flux and for high heat fluxes, the heat transfer will be really based on the vapotron effect, *i.e.*, vaporization and condensation phenomena at the wall. For higher mass fluxes, the heat transfer is controlled by the movement of the liquid due to the creation of vortices in the inter-fin space. Further tests are necessary to confirm this tendency if this geometry is used for fusion application. On Fig. 7, it is also shown a very slight effect of the pressure on the Incident CHF.

3.5. Comparison between the geometries

These different cooling structures show a good efficiency in terms of Incident CHF because they are able to remove about 20 - 25 MW/m^2, depending on well selected thermal hydraulic conditions. As expected, the mass flux is the main factor acting on the CHF for the different geometries within the investigated range. The best result was obtained with the externally finned swirl tube: ICHF = 45.8 MW/m^2, G = 20 Mg.m^{-2}.s^{-1}, T_{in} = 22°C, P = 1 MPa. The comparison between the different

geometries is shown in Fig. 9. It is noticed an increase of the Incident CHF with reference to a smooth tube. For G = 10 $Mg.m^{-2}.s^{-1}$, the enhancement factor is 1.16 for hypervapotron, 1.41 for M7 screw tube and 1.59 for externally finned swirl tube. Another approach is to consider a given Incident CHF. To reach an Incident CHF of 25 MW/m^2 at constant pressure, P = 1 MPa, and inlet temperature, T_{in} = 30°C, a smooth tube requires G = 12 $Mg.m^{-2}.s^{-1}$, a hypervapotron G = 10 $Mg.m^{-2}.s^{-1}$, a M7 screw tube and an externally finned swirl tube G = 6 $Mg.m^{-2}.s^{-1}$. More generally, ICHF of a screw tube is 1.5 higher than a smooth tube, within the experimental range.

The other experimental result that characterizes the efficiency of a cooling concept is the pressure drop. The comparison between the different geometries is presented in Fig. 10, where the lineic pressure drop, *i.e.*, normalized by one meter, of the test sample is plotted versus the mass flux at room temperature. Externally finned swirl tube and M7 screw tube show equivalent results: a lineic pressure drop about three times larger than for smooth tube. Hypervapotron produces the highest lineic pressure drop, but this result also includes local pressure drop due to inlet and outlet connection regions, which were not optimized (Ref. 8).

Finally, as a basic approach to determine the best cooling geometry, the Incident CHF is plotted versus the lineic pumping power in Fig. 11. The main point is the similar performance between externally finned swirl tube and M7 screw tube. It can also be noticed that smooth tube shows a rather good efficiency due to a lower pressure drop. Hypervapotron does not appear as very efficient according to these results.

These tests confirm the predominant efficiency of swirl and screw tubes in terms of incident CHF as well as in terms of pumping power. It appears to be of interest to perform new experiments to optimize screw geometry by evaluating the effect of pitch, fin height and shape. As a design approach, manufacturing process has to be considered. The twisted-tape inserted inside the channel of the tube may be properly connected to the walls to avoid important pressure drop. Screw tube appears to be the easiest tube to manufacture if other material, except OFHC-Cu that is too soft, are considered as copper alloys, for example.

4. ANALYSIS OF EXPERIMENTAL RESULTS

During tests, tubes are only one-side heated by an incident heat flux that is determined from experiments. However, the dry-out of the inner wall is not directly controlled by this heat flux. It may be reasonably expected that the dry-out phenomenon, which is responsible for the CHF occurrence, is directly related to the maximum wall flux. Thus, the analysis of the results requires to determine the maximum wall CHF from the incident CHF. It may be obtained by solving the heat conduction in the material, provided that boundary conditions at the inner wall are known. This process requires the calculation of the heat transfer coefficient at the inner wall in the convective and in the subcooled boiling regimes.

Heat transfer correlations are only available for one-side heating conditions for smooth and swirl tubes for these different regimes (Ref. 9):

- forced convection regime: Dittus-Boelter correlation multiplied by a viscosity factor

$$Nu = (\mu/\mu_w)^{0.14} \times 0.023\, Re^{0.8}\, Pr^{0.4} \qquad \text{(Eq. 1)}$$

where Nu = h ID /k is the Nusselt number, Re = G ID / μ the Reynolds number and Pr the Prandtl number.

- subcooled boiling: JAERI correlation

$$T_w - T_{sat} = 25.72\, \Phi^{1/3}\, e^{-P/8.6} \qquad \text{(Eq. 2)}$$

In this expression, P [MPa] and Φ [MW/m^2].

- connection convection / subcooled boiling regimes: Bergles & Rohsenow method

$$\Phi^2_{\text{partial boiling}} = \Phi^2_{\text{convection}} + \left(\Phi_{\text{boiling}} - \Phi_{ONB}\right)^2 \qquad \text{(Eq. 3)}$$

- Onset of Nucleate Boiling (ONB) temperature: Bergles & Rohsenow equation

$$T_{ONB} - T_{sat} = 0.556 \left[\frac{\Phi_{ONB}}{1082(10P)^{1.156}} \right]^{0.463(10P)^{0.0234}} \qquad \text{(Eq. 4)}$$

In this expression, P [MPa] and Φ [W/m^2].

An example of the evolution of the heat transfer coefficient versus the wall temperature is given in Fig. 12.

The evolution of the wall temperature is obtained from 2D steady state finite element (FE) calculations with ABAQUS code. The wall heat flux is deduced from the wall temperature by:

$$\Phi_w = h(T_w)(T_w - T_f) \qquad \text{(Eq. 5)}$$

Evolutions of the temperature and the heat flux at the wall are presented in Fig. 13 to Fig. 21 for smooth tube and in Fig. 22 to Fig. 36 for externally finned swirl tube. The origin of the angle corresponds to the top of the inner wall. The onset of nucleate boiling, T_{onb}, temperature indicates the limit between the convective regime and the subcooled boiling regime. According to calculations, the subcooled boiling regime occurs at the upper part of the tube. It is also shown a non homogeneous distribution of the temperature and of the heat flux at the wall. Maxima are reached at the top of the inner wall.

For smooth tube, calculations reveal that the maximum temperature at the inner wall is constant, 240-250°C, whatever the mass flux, the pressure and the temperature. The part of the wall in the subcooled boiling regime seems also to be constant. It represents an average angle percentage of 40% of the circumference, as shown by Fig. 37, or an angle of 145° as illustrated by Fig. 38.

For externally finned swirl tube, calculations show that the maximum temperature at the inner wall always remains in the range 250-270°C, which is a little bit higher than the maximal temperature of smooth tube. This is an advantage of this geometry. Temperature and heat flux do not decrease continuously. A first local minimum of both temperature and heat flux occurs for a constant angle of 95-100° that corresponds to the transition between the circular profile and the external fin profile. As shown in Fig. 39, the percentage of the inner wall in the subcooled boiling regime depends on the mass flux and on the pressure. The forced convection regime appears at the inner wall from $G = 6\ Mg.m^{-2}.s^{-1}$ for $P = 1.5$ MPa and for $P = 1$ MPa. For $P = 1.5$ MPa, the percentage in subcooled boiling regime decreases significantly from $G = 12\ Mg.m^{-2}.s^{-1}$. For $P = 1$ MPa, this significant decrease begins from $G = 16\ Mg.m^{-2}.s^{-1}$.

For hypervapotron and screw tube, heat transfer correlations are not available so far. Thus, such an analysis appears to be impossible at present.

Thermal hydraulic results are summarized in Table 1 for smooth tube, in Table 2 for externally finned swirl tube, in Table 3 for screw tubes and in Table 4 for hypervapotron. The subscript 'local' means 'at the CHF location'.

5. CHF MODELING

For smooth tube, the modification of Tong 68 correlation (Ref. 10) proposed by Inasaka et Nariai (Ref. 11) is used:

$$\Phi_c / i_{LV} = C G^{0.4} \mu_{sat}^{0.6} / ID^{0.6}$$

$$C/C_{Tong\,68} = 1 - \left[\left(52.3 + 80\,x_{local} - 50\,x_{local}^2\right) \Big/ \left(60.5 + \left(10^{-5} P_{local}\right)^{1.4}\right) \right] \quad \text{(Eq. 6)}$$

$$C_{Tong\,68} = 1.76 - 7.433 x_{local} + 12.222 x_{local}^2$$

Fig. 40 shows that Inasaka et Nariai correlation predicts in a ±20% range experimental results.

For externally finned swirl tube, modified correlation proposed by Ref. 13 based on Tong 75 correlation (Ref. 12) is used:

$$Bo_{SW} = 1.67 \exp(x) \times 1.84 \left(D/D_0\right)^{0.32} Re_{Dh}^{-0.6} \left[1 + 0.00216 \left(P/P_C\right)^{1.8} Re_{Dh}^{0.5}\, Ja\right] \quad \text{(Eq. 7)}$$

where $Bo_{SW} = \Phi_C / (\rho\, V_{SW}\, i_{LV})$ is the Boiling number based on the swirl velocity V_{SW} and $Re_{Dh} = G\, Dh / \mu$ the Reynolds number based on the hydraulic diameter Dh. The swirl velocity is defined as

$$V_{SW} = \sqrt{1 + \left(\pi / 2T_R\right)^2}\, V_{axial} \quad \text{(Eq. 8)}$$

where T_R is the twist ratio. It is the number of inner diameter in a 180° twist. The hydraulic diameter is

$$Dh = 4 \frac{\left(\pi ID^2/4\right) - t_{SW}\, ID}{\pi ID + 2ID - 2t_{SW}} \quad \text{(Eq. 9)}$$

where t_{SW} is the thickness of the twisted tape.

For hypervapotron and screw tube, heat transfer correlations are not available so far. Thus, such an analysis appears to be impossible at present.

Thermal hydraulic results are summarized in Table 1 for smooth tube, in Table 2 for externally finned swirl tube, in Table 3 for screw tubes and in Table 4 for hypervapotron. The subscript 'local' means 'at the CHF location'.

5. CHF MODELING

For smooth tube, the modification of Tong 68 correlation (Ref. 10) proposed by Inasaka et Nariai (Ref. 11) is used:

$$\Phi_c / i_{LV} = C G^{0.4} \mu_{sat}^{0.6} / ID^{0.6}$$

$$C/C_{Tong\,68} = 1 - \left[\left(52.3 + 80\,x_{local} - 50\,x_{local}^2\right) \Big/ \left(60.5 + \left(10^{-5} P_{local}\right)^{1.4}\right) \right] \quad \text{(Eq. 6)}$$

$$C_{Tong\,68} = 1.76 - 7.433 x_{local} + 12.222 x_{local}^2$$

Fig. 40 shows that Inasaka et Nariai correlation predicts in a ±20% range experimental results.

For externally finned swirl tube, modified correlation proposed by Ref. 13 based on Tong 75 correlation (Ref. 12) is used:

$$Bo_{SW} = 1.67 \exp(x) \times 1.84 \left(D/D_0\right)^{0.32} Re_{Dh}^{-0.6} \left[1 + 0.00216 \left(P/P_C\right)^{1.8} Re_{Dh}^{0.5}\, Ja\right] \quad \text{(Eq. 7)}$$

where $Bo_{SW} = \Phi_C / (\rho\, V_{SW}\, i_{LV})$ is the Boiling number based on the swirl velocity V_{SW} and $Re_{Dh} = G\, Dh / \mu$ the Reynolds number based on the hydraulic diameter Dh. The swirl velocity is defined as

$$V_{SW} = \sqrt{1 + \left(\pi / 2T_R\right)^2}\, V_{axial} \quad \text{(Eq. 8)}$$

where T_R is the twist ratio. It is the number of inner diameter in a 180° twist. The hydraulic diameter is

$$Dh = 4 \frac{\left(\pi ID^2/4\right) - t_{SW}\, ID}{\pi ID + 2ID - 2t_{SW}} \quad \text{(Eq. 9)}$$

where t_{SW} is the thickness of the twisted tape.

As shown in Fig. 41, the proposed correlation predicts with ±20% accuracy the experimental results.

6. CONCLUSION

This report is a complete analysis of the CHF tests performed by JAERI in the frame of the design of high heat flux components for ITER. Different geometries were tested using the same facility of JAERI: smooth tube, externally finned swirl tube, screw tube and hypervapotron. Experimental results show that the mass flux or the velocity is the main parameter acting on CHF. It is confirmed that externally finned swirl tubes are an efficient means of removing high heat fluxes. It is also shown that screw tubes can reach the same performance as swirl tube, within the experimental range. Finite element calculations revealed a non homogeneous distribution of the temperature and the heat flux at the wall for smooth and externally finned swirl tube. For smooth tube, the angle percentage in subcooled boiling regime seems independant from thermal hydraulic conditions such as the velocity. It is shown that an external fin allows the subcooled boiling regime to be reached on a large part of the wall. For this geometry, the angle percentage in subcooled boiling regime depends on the velocity and the pressure. Test results were compared with Inasaka et Nariai correlation for smooth and modified correlation for externally finned swirl tubes. Experimental results are predicted with ±20% accuracy.

As shown in Fig. 41, the proposed correlation predicts with ±20% accuracy the experimental results.

6. CONCLUSION

This report is a complete analysis of the CHF tests performed by JAERI in the frame of the design of high heat flux components for ITER. Different geometries were tested using the same facility of JAERI: smooth tube, externally finned swirl tube, screw tube and hypervapotron. Experimental results show that the mass flux or the velocity is the main parameter acting on CHF. It is confirmed that externally finned swirl tubes are an efficient means of removing high heat fluxes. It is also shown that screw tubes can reach the same performance as swirl tube, within the experimental range. Finite element calculations revealed a non homogeneous distribution of the temperature and the heat flux at the wall for smooth and externally finned swirl tube. For smooth tube, the angle percentage in subcooled boiling regime seems independant from thermal hydraulic conditions such as the velocity. It is shown that an external fin allows the subcooled boiling regime to be reached on a large part of the wall. For this geometry, the angle percentage in subcooled boiling regime depends on the velocity and the pressure. Test results were compared with Inasaka et Nariai correlation for smooth and modified correlation for externally finned swirl tubes. Experimental results are predicted with ±20% accuracy.

Acknowledgment

Dr. J. Boscary would like to acknowledge the Science and Technology Agency of Japan that supports his fellowship in the NBI Heating Laboratory. The authors would like to acknowledge Dr Y. Okumura, Dr. M. Ohta and Dr. H. Kishimoto of JAERI for their support and encouragement. The authors would like to acknowledge also Dr S. Suzuki of NBI heating laboratory and Dr. W. Hashimoto of Nikon Systems Co. Ltd. for their valuable comments and assistance on the finite element calculations.

REFERENCES

Ref. 1 M. Araki, M Dairaku, T. Inoue, M. Komata, M. Kuriyama, S. Matsuda, M. Ogawa, Y. Ohara, M. Seki, K. Yokoyama 1989
Burnout experiments on the externally finned swirl tube for steady-state and high heat flux beam stops, Fusion Eng. Des. 9, 231-236

Ref. 2 M. Araki, T.D. Watson, T.D. Marshall, P.D. Rockett, M. Akiba 1994
Effect of subcooling on the critical heat flux under one-side heating conditions, 18th SOFT, Karlsruhe, 1, 251-254

Ref. 3 C.B. Baxi 1993
Evaluation of helium cooling for fusion divertor, GA-A21448, General Atomics

Ref. 4 H.D. Falter, E. Thompson 1996
Performance of hypervapotron beam stopping elements at JET, Fusion Tech., 584-595

Ref. 5 J.A. Koski, A.G. Beattie, J.B. Whitley, C.D. Croesmann 1987
Experimental verification of subcooled flow boiling for Tokamak pump limiter designs, Nat. Heat Transf. Conf., Pittsburgh ASME, 87-HT-45

Ref. 6 J. Schlosser, J. Boscary 1993
Thermalhydraulic tests at NET/ITER relevant conditions on divertor targets using swirl tubes, NURETH 6, Grenoble France, 815-824

Ref. 7 J. Schlosser, J. Boscary, F. Escourbiac, I. Smid, G. Vieider 1996
Comparison between various thermal hydraulic tube concepts for the ITER divertor, SOFT 19, Lisbonna, Portugal

Ref. 8 M. Araki, K. Sato, S. Suzuki, M. Akiba 1996
Critical heat flux experiment on the screw tube under one-side heating conditions, Fusion Technology 29, 519-528.

Ref. 9 M. Araki, M. Ogawa, T. Kunugi, K. Satoh, S. Suzuki 1996
Experiments on heat transfer of smooth and swirl tubes under one-side heating conditions, Int. J. Heat Mass Transfer 39(14) 3045-3055.

Ref. 10 L.S. Tong 1968

Boundary layer analysis of the flow boiling crisis, Int. J. Heat Mass Transfer 11 1208-1211

Ref. 11 Inasaka F., Nariai H. 1987

Critical heat flux and flow characteristics of subcooled flow boiling in narrow tubes, JSME Int. J., 30, 268.

Ref. 12 L. S. Tong 1975

A phenomenological study of critical heat flux, ASME paper 75-HT-68.

Ref. 13 J. Boscary 1995

Transfert thermique et flux critique dans un écoulement hélicoïdal en tube chauffé asymétriquement, Ph.D thesis, Institut National Polytechnique de Toulouse.

NOMENCLATURE

$Bo = \Phi / (\rho V i_{LV})$

C_P specific heat at constant pressure [$J.kg^{-1}.C^{-1}$]

Dh hydraulic diameter [m]

G mass flux [$kg.m^{-2}.s^{-1}$], 1 $Mg.m^{-2}.s^{-1}$ = 1000 $kg.m^{-2}.s^{-1}$

h heat transfer coefficient [$W.m^{-2}.C^{-1}$]

ID internal diameter [m]

i_{LV} vaporization latent heat [J/kg]

$Ja = (\rho_L / \rho_V) [C_P(T_{sat} - T)] / i_{LV}$ Jakob number [dimensionless]

k conductivity [$W.m^{-1}.C^{-1}$]

$Nu = h\ ID / k$ Nusselt number [dimensionless]

OD outer diameter [m]

P pressure [MPa]

Pr Prandtl number [dimensionless]

$Re = G\ ID / \mu$ Reynolds number [dimensionless]

t thickness [m]

T temperature [°C]

T_R twist ratio [dimensionless]

V velocity [m/s]

$x = - C_P \Delta T_{sub} / i_{LV}$ mass enthalpic quality

Φ heat flux [W/m^2]

μ dynamic viscosity [$kg.m^{-1}.s^{-1}$]

ρ density [kg/m^3]

Subscripts

in inlet

sat saturation

sw swirl

w wall

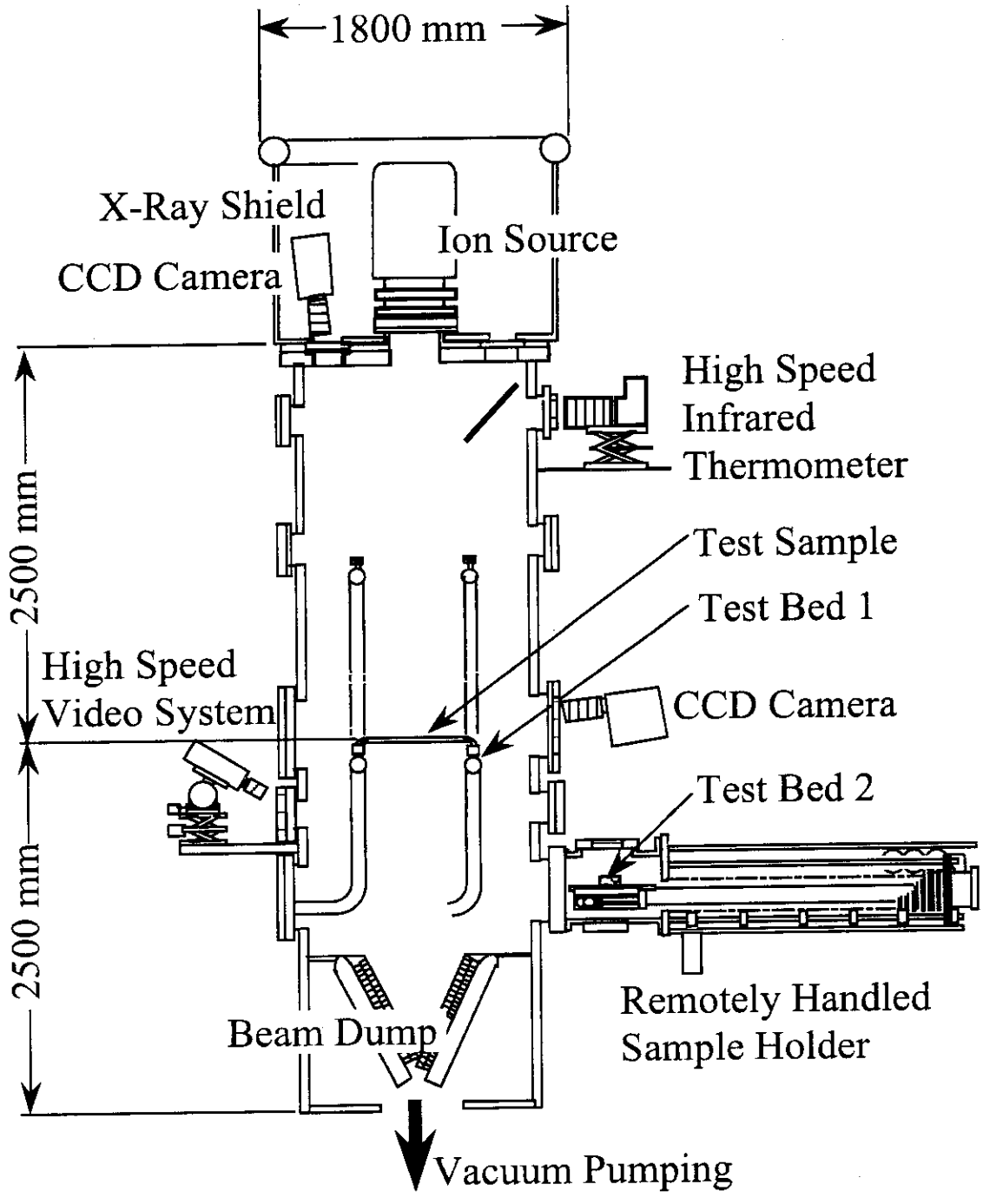

Figure 1: PBEF facility

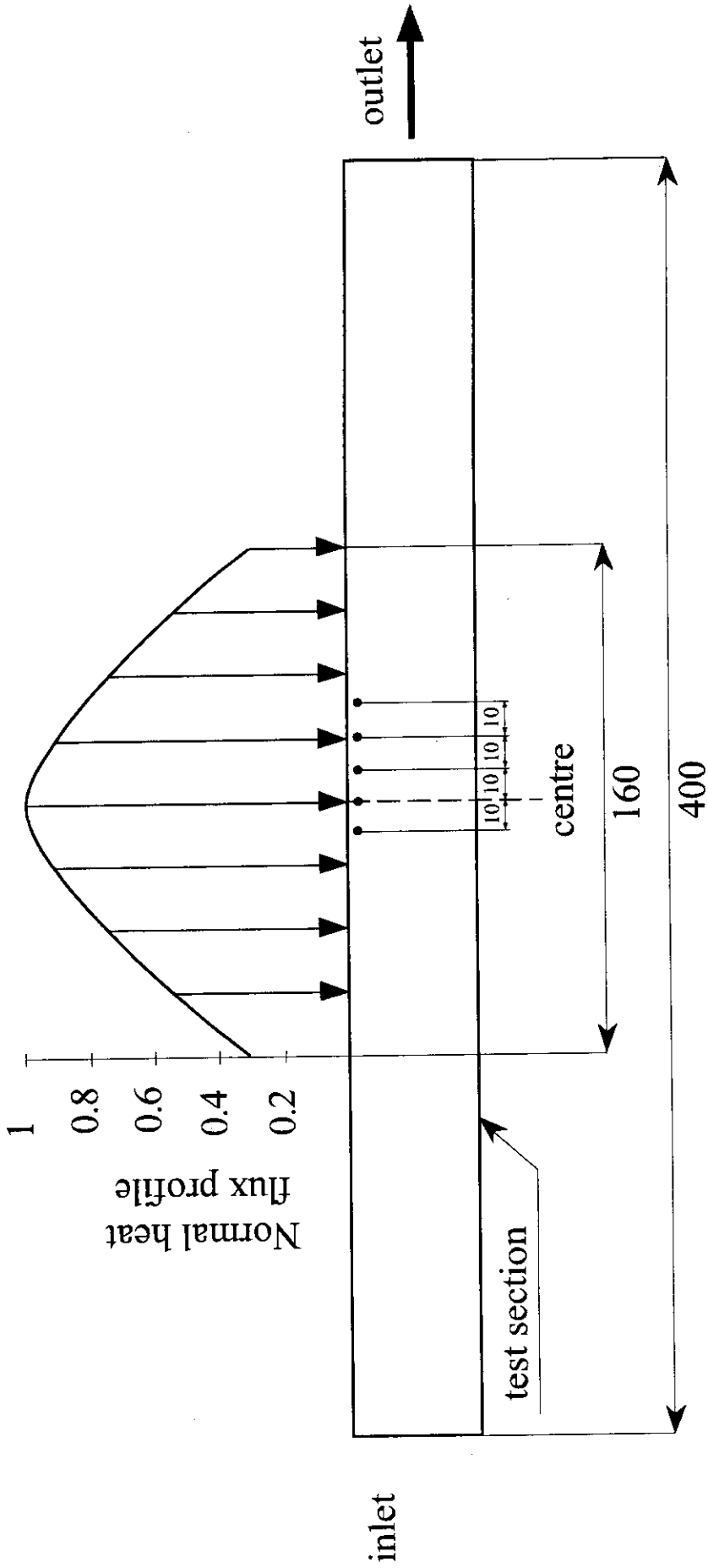

Figure 2: Experimental conditions

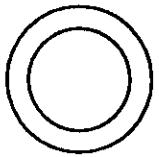

Smooth tube
Material: OFHC-Cu
Outer diameter: 10 mm
Inner diameter: 7 mm

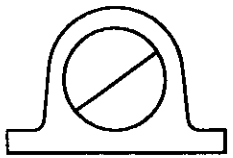

Externally-finned swirl tube
Material: OFHC-Cu
Outer diameter: 10 mm
Inner diameter: 7 mm
External fin width: 15 mm
External fin height: 3 mm
Tape material: Iconel-625
Tape twist ratio: 3
Tape thickness: 0.35 mm

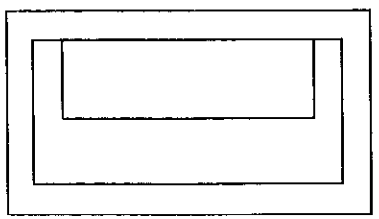

Hypervapotron
Material: OFHC-Cu
Width: 25 mm
Height: 14 mm
Wall thickness: 2.5 mm
Fin width: 14 mm
Fin height: 4 mm
Fin thickness: 3 mm
Inter-fin gap: 3 mm

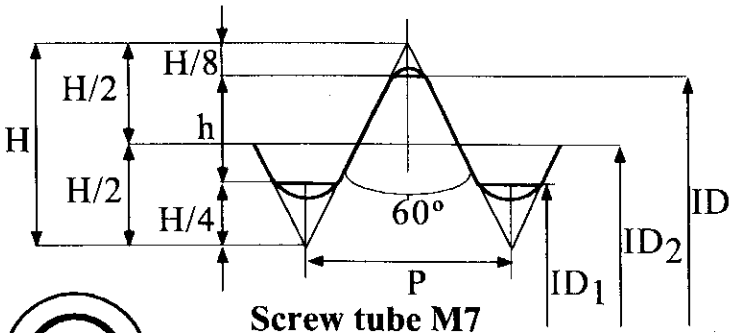

B 0205

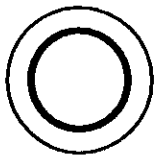

Screw tube M7
Material: OFHC-Cu
ID = 7 mm Outer diameter: 10 mm
ID2 = 6.35 mm ID1 = 5.91 mm
Pitch: 1 mm Fin height: 0.87 mm

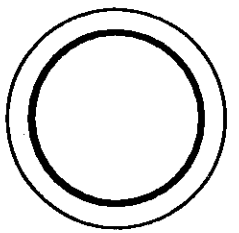

Screw tube M12
Material: OFHC-Cu
ID = 12 mm Outer diameter: 15 mm
ID2 = 10.86 mm ID1 = 10.11 mm
Pitch: 1.75 mm Fin height: 1.51 mm

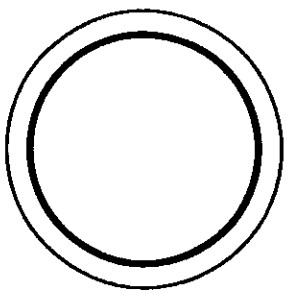

Screw tube M16
Material: OFHC-Cu
ID = 16 mm Outer diameter: 19 mm
ID2 = 14.70 mm ID1 = 13.84 mm
Pitch: 2 mm Fin height: 1.73 mm

Figure 3: Geometrical characteristics of the test sections

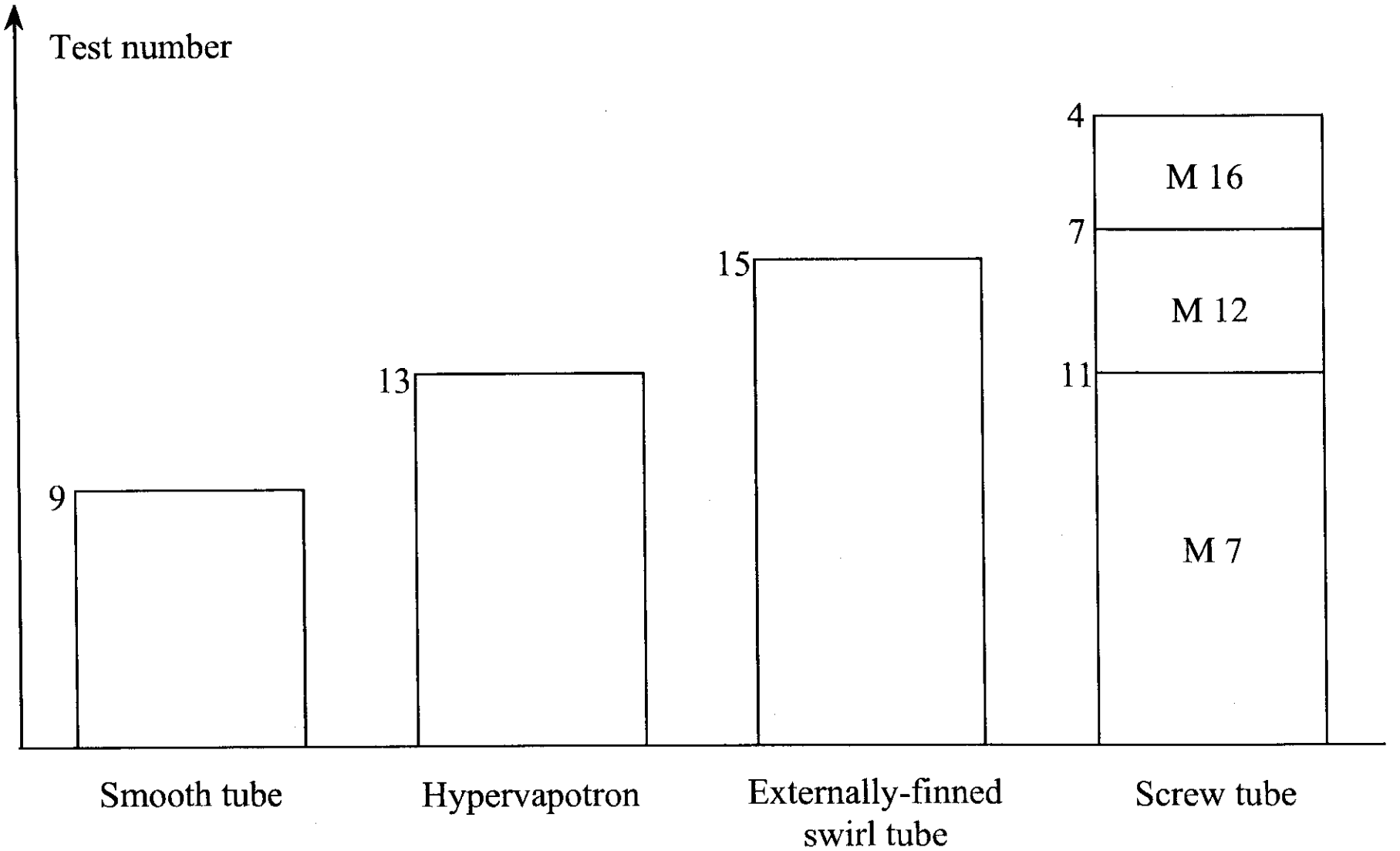

Figure 4: Distribution of the test number between the different geometries

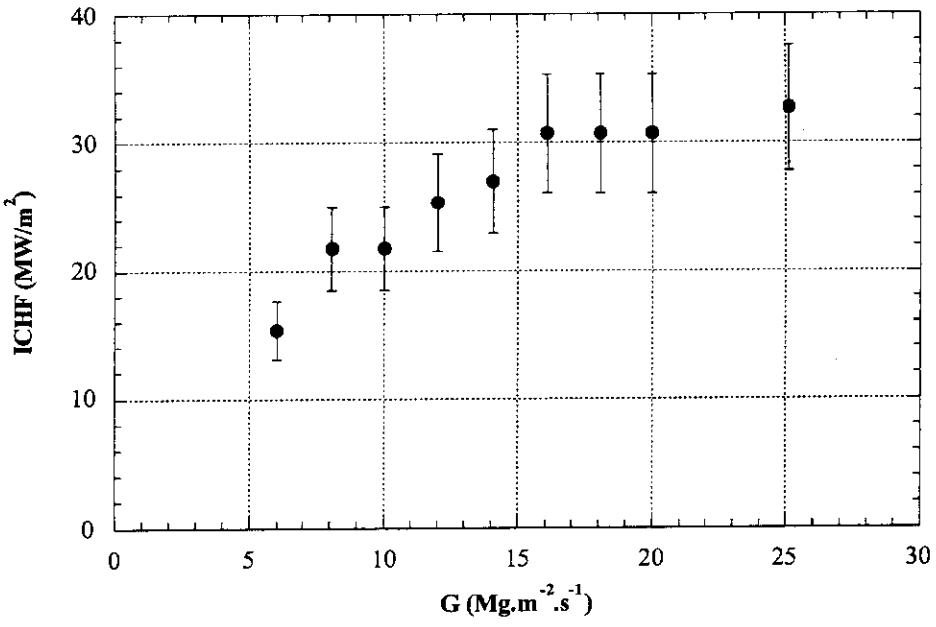

Figure 5: Incident CHF versus mass flux for smooth tube
(T_{in} = 30°C, P = 1 MPa)

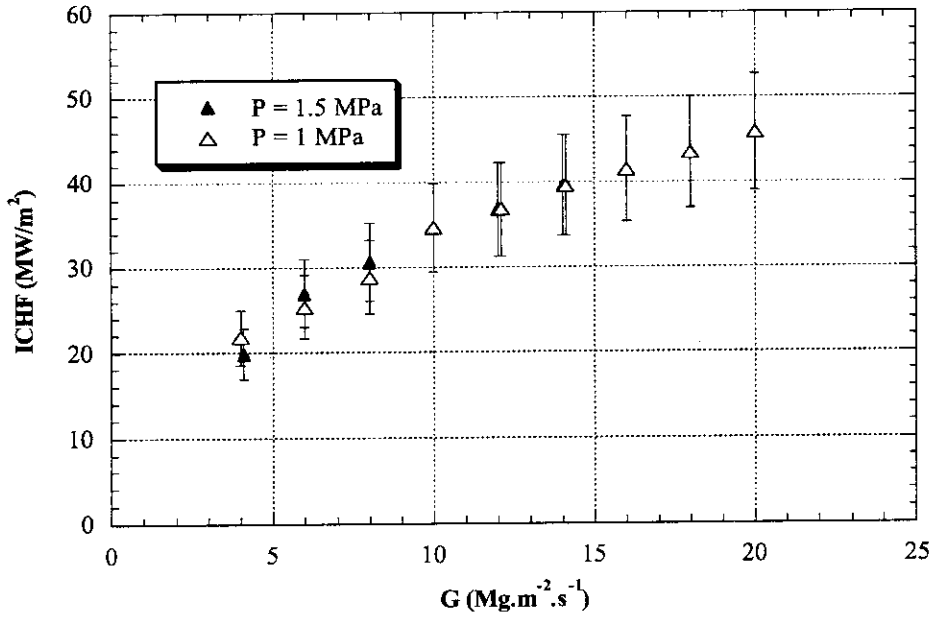

Figure 6: Incident CHF versus mass flux for externally-finned swirl
(Tin = 25°C)

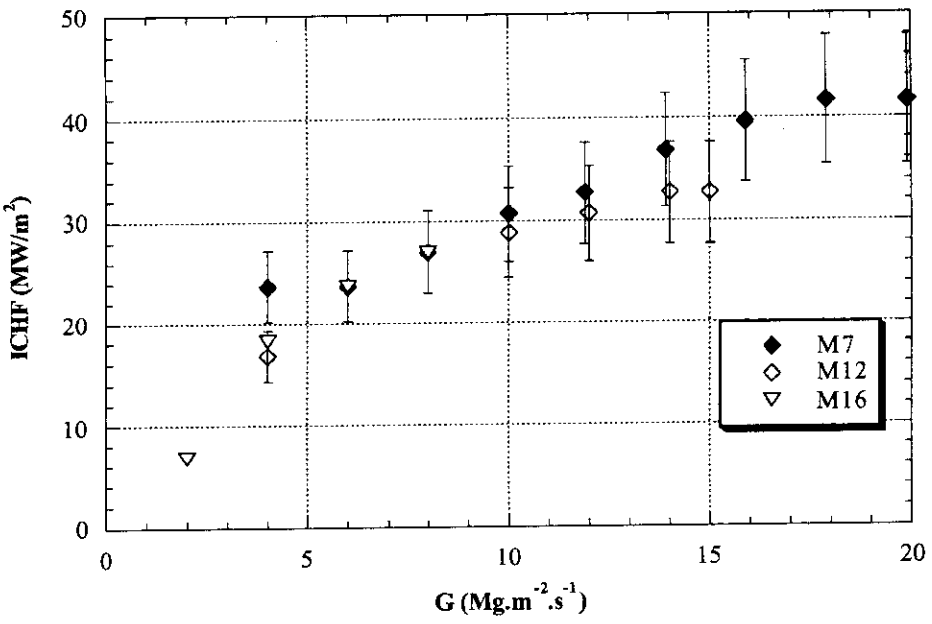

Figure 7: Incident CHF versus mass flux for screw tube
(T_{in} = 30°C, P = 1 MPa)

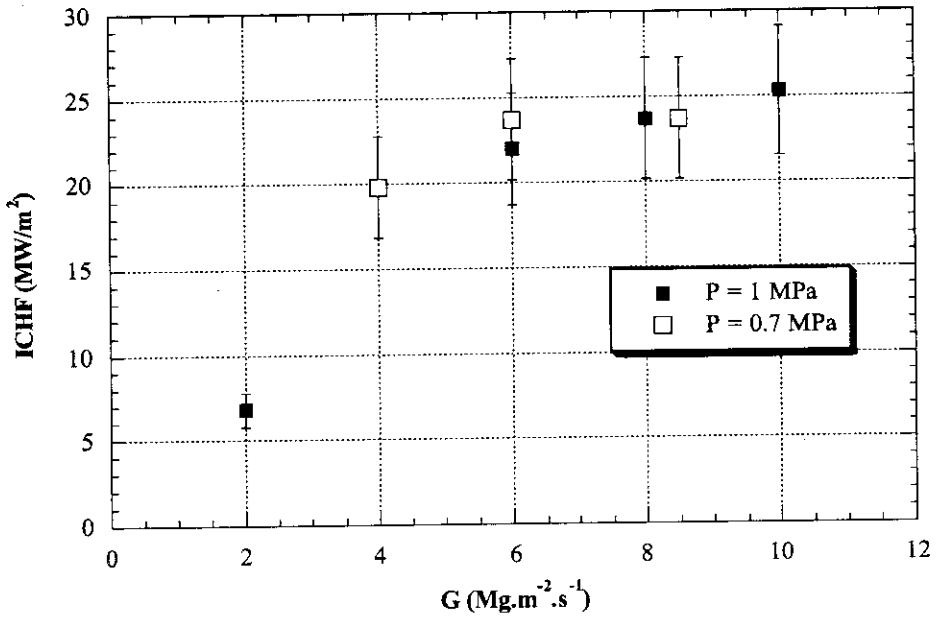

Figure 8: Incident CHF versus mass flux flux for hypervapotron
(T_{in} = 30°C)

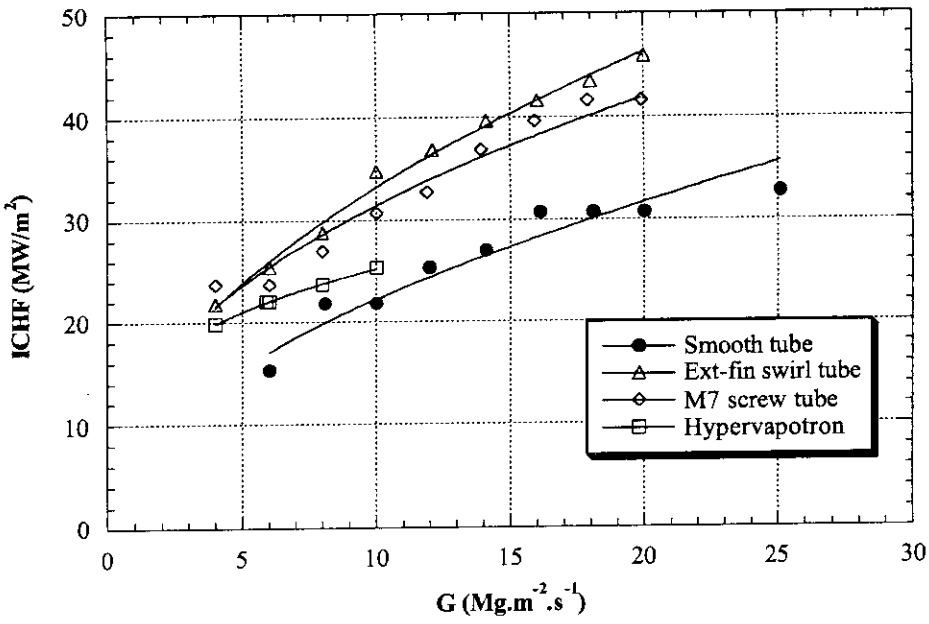

Figure 9: Incident CHF versus mass flux for the different geometries
(P = 1 MPa, T_{in} = 25-30°C)

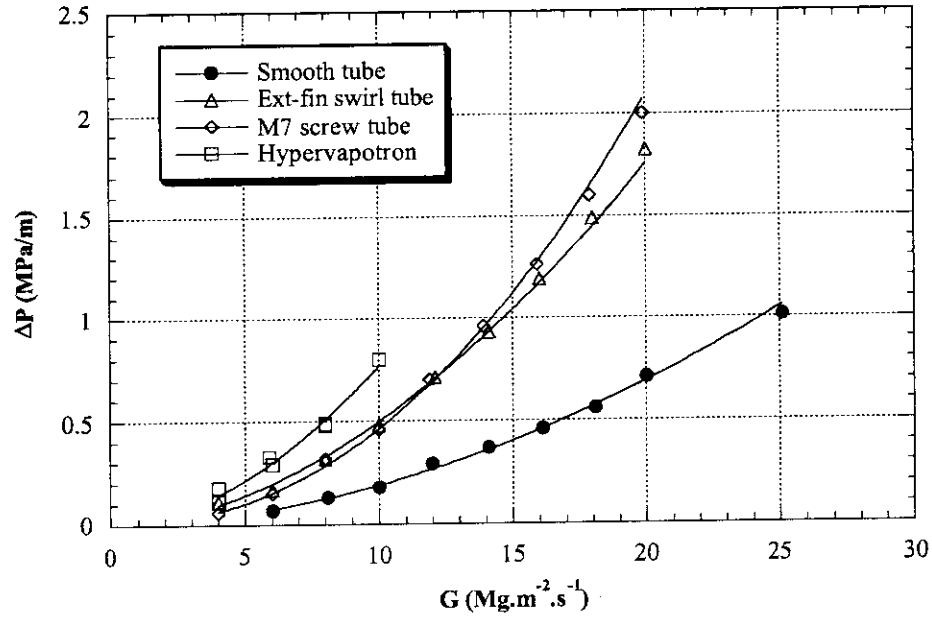

Figure 10: Lineic pressure drop versus mass flux for the different geometries
(P = 1 MPa, T_{in} = 25-30°C)

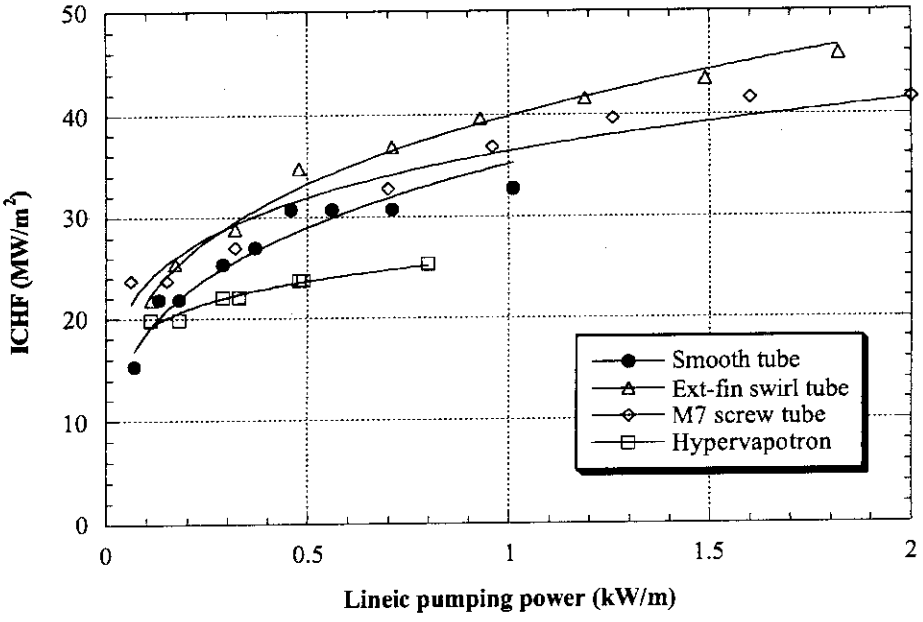

Figure 11: ICHF versus lineic pumping power for the different geometries
(P = 1 MPa, T_{in} = 25-30°C)

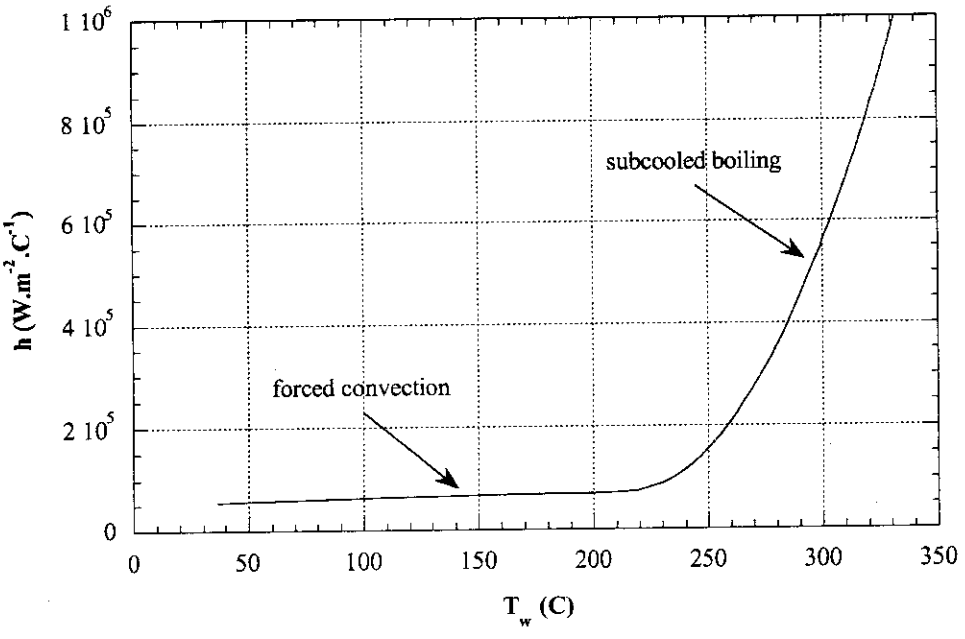

Figure 12: Heat transfer coefficient versus wall temperature
(T_{in} = 28°C, P = 1 MPa, G = 16.1 Mg.m^{-2}.s^{-1})

Geometry and transversal incident flux profile	Longitudinal incident flux profile	L_h (mm)	P_{in} (MPa)	P_{out} (MPa)	P_{local} (MPa)	T_{in} (°C)	T_{out} (°C)	T_{local} (°C)	T_{sat}-T_{local} (°C)	G ($Mg.m^{-2}.s^{-1}$)	V_{axial} (m/s)	ΔP_{lineic} (MPa/m)	ICHF (MW/m^2)	Eng. WCHF (MW/m^2)	FE WCHF (MW/m^2)	FE peaking factor	Shot number
1996 **JAERI** OFHC-Cu OD = 10 mm ID = 7 mm PBEF Ion Beam Eng. Peaking factor: 1.43	1 0.3 0 $L_h/2$ L_h	160	1.3	0.9	1.0	30	41	36	143	25.1	25	1.01	32.7	46.7	41.5	1.27	E59

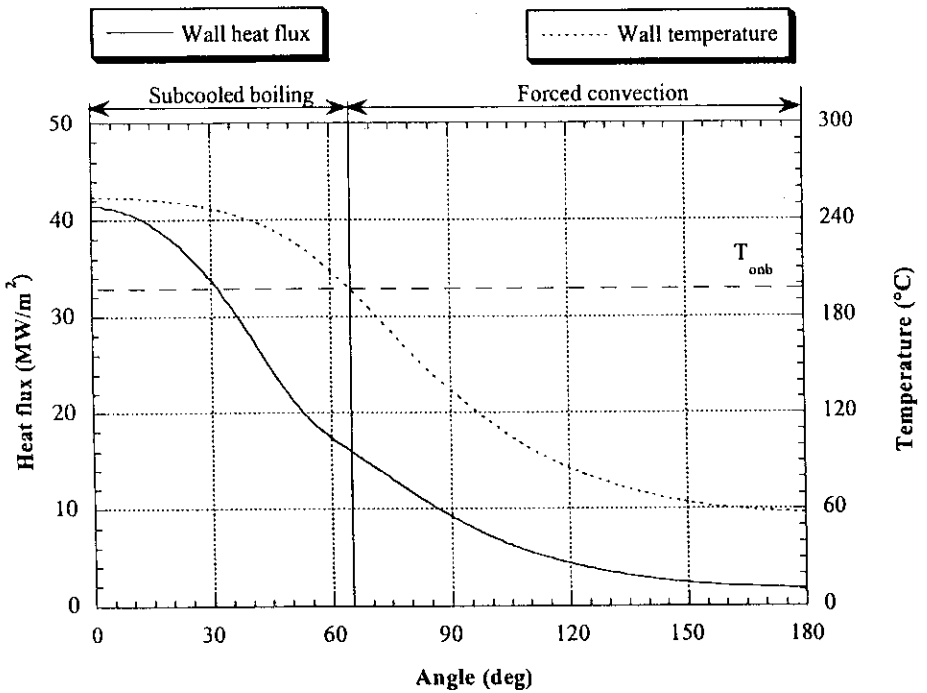

Fig. 13: Thermal hydraulic conditions and heat transfer analysis of test E59

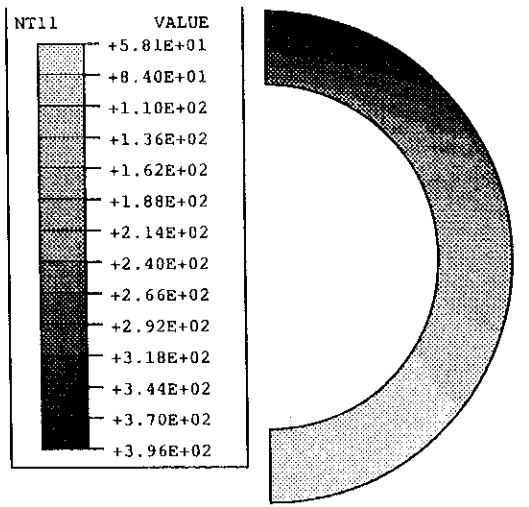

Isotherms in the material

Geometry and transversal incident flux profile	Longitudinal incident flux profile	L_h (mm)	P_{in} (MPa)	P_{out} (MPa)	P_{local} (MPa)	T_{in} (°C)	T_{out} (°C)	T_{local} (°C)	T_{sat}-T_{local} (°C)	G ($Mg.m^{-2}.s^{-1}$)	V_{axial} (m/s)	ΔP_{fineic} (MPa/m)	ICHF (MW/m^2)	Eng. WCHF (MW/m^2)	FE WCHF (MW/m^2)	FE peaking factor	Shot number
1996 JAERI OFHC-Cu OD = 10 mm ID = 7 mm PBEF Ion Beam Eng. Peaking factor: 1.43	1 0.3 0 $L_h/2$ L_h	160	1.26	0.9	1.0	30	43	37	142	20.0	20	0.71	30.7	46.7	39.1	1.27	E54

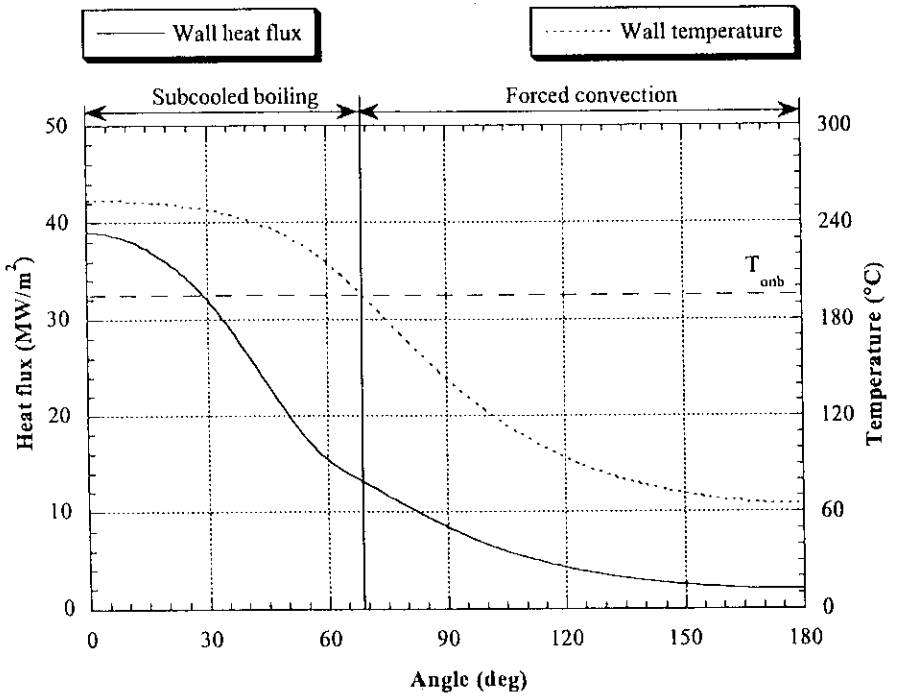

Fig. 14: Thermal hydraulic conditions and heat transfer analysis of test E54

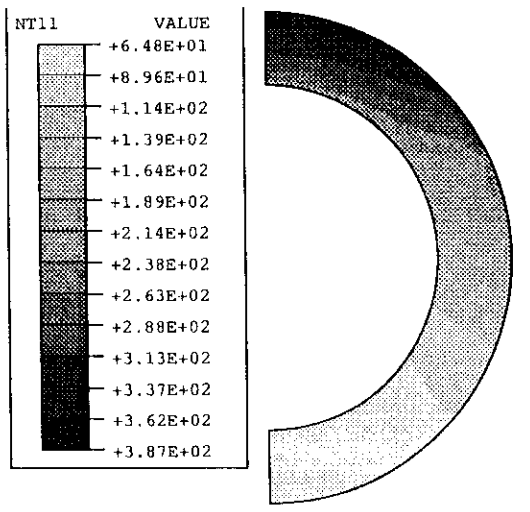

Isotherms in the material

Geometry and transversal incident flux profile	Longitudinal incident flux profile	L_h (mm)	P_{in} (MPa)	P_{out} (MPa)	P_{local} (MPa)	T_{in} (°C)	T_{out} (°C)	T_{local} (°C)	T_{sat}-T_{local} (°C)	G ($Mg.m^{-2}.s^{-1}$)	V_{axial} (m/s)	ΔP_{lineic} (MPa/m)	ICHF (MW/m^2)	Eng. WCHF (MW/m^2)	FE WCHF (MW/m^2)	FE peaking factor	Shot number
1996 **JAERI** OFHC-Cu OD = 10 mm ID = 7 mm PBEF Ion Beam Eng. Peaking factor: 1.43	1 0.3 0 $L_h/2$ L_h	160	1.23	0.9	1.0	28	42	35	144	18.1	18	0.56	30.7	43.9	39.1	1.27	E47

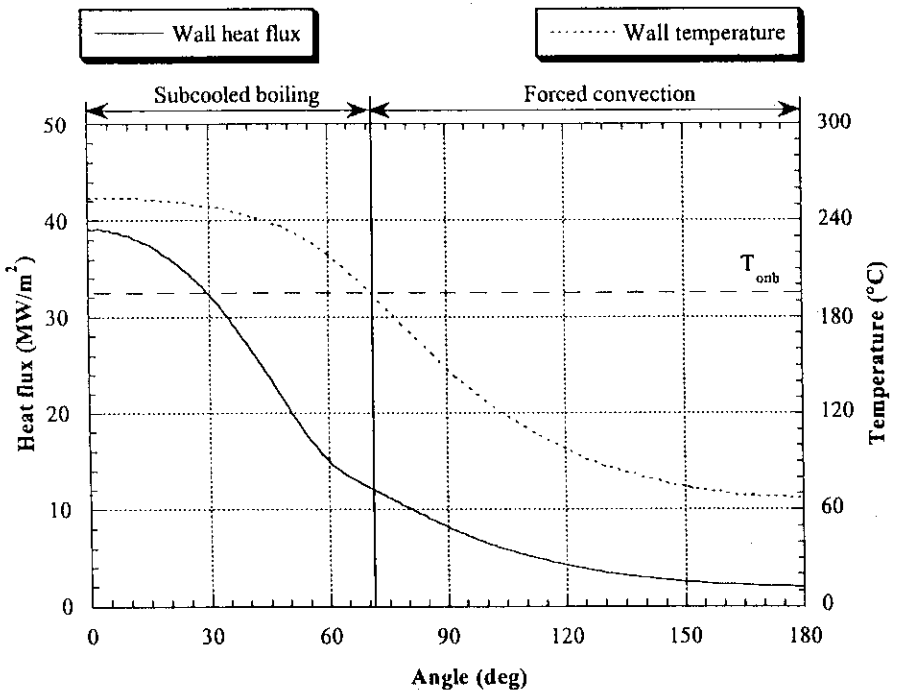

Fig. 15: Thermal hydraulic conditions and heat transfer analysis of test E47

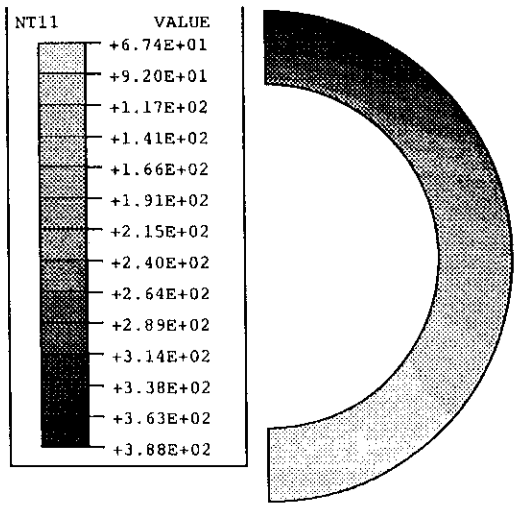

Isotherms in the material

Geometry and transversal incident flux profile	Longitudinal incident flux profile	L_h (mm)	P_{in} (MPa)	P_{out} (MPa)	P_{local} (MPa)	T_{in} (°C)	T_{out} (°C)	T_{local} (°C)	T_{sat}-T_{local} (°C)	G ($Mg.m^{-2}.s^{-1}$)	V_{axial} (m/s)	ΔP_{lineic} (MPa/m)	ICHF (MW/m^2)	Eng. WCHF (MW/m^2)	FE WCHF (MW/m^2)	FE peaking factor	Shot number
1996 JAERI OFHC-Cu OD = 10 mm ID = 7 mm PBEF Ion Beam Eng. Peaking factor: 1.43	1 0.3 0 $L_h/2$ L_h	160	1.2	0.9	1.0	28	45	37	142	16.1	16	0.46	30.7	43.9	39.1	1.27	E38

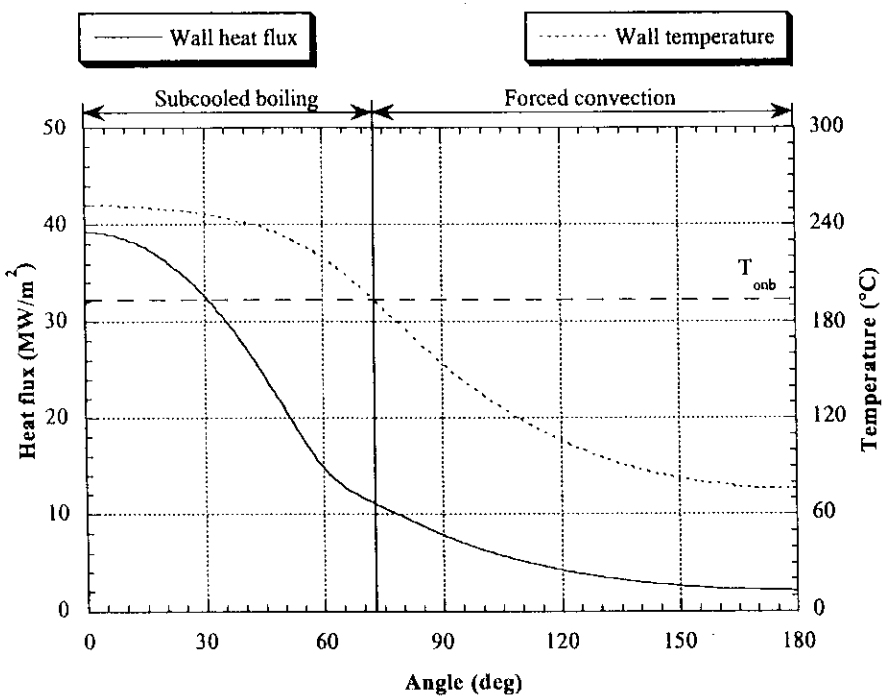

Fig. 16: Thermal hydraulic conditions and heat transfer analysis of test E38

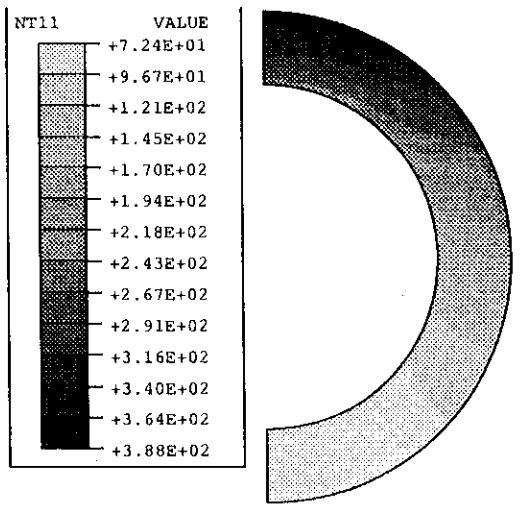

Isotherms in the material

Geometry and transversal incident flux profile	Longitudinal incident flux profile	L_h (mm)	P_{in} (MPa)	P_{out} (MPa)	P_{local} (MPa)	T_{in} (°C)	T_{out} (°C)	T_{local} (°C)	$T_{sat}-T_{local}$ (°C)	G ($Mg.m^{-2}.s^{-1}$)	V_{axial} (m/s)	ΔP_{lineic} (MPa/m)	ICHF (MW/m^2)	Eng. WCHF (MW/m^2)	FE WCHF (MW/m^2)	FE peaking factor	Shot number
1996 **JAERI** OFHC-Cu OD = 10 mm ID = 7 mm PBEF Ion Beam Eng. Peaking factor: 1.43	1 0.3 0 $L_h/2$ L_h	160	1.2	1.0	1.0	28	45	37	142	14.1	14	0.37	27.0	38.6	34.5	1.28	E44

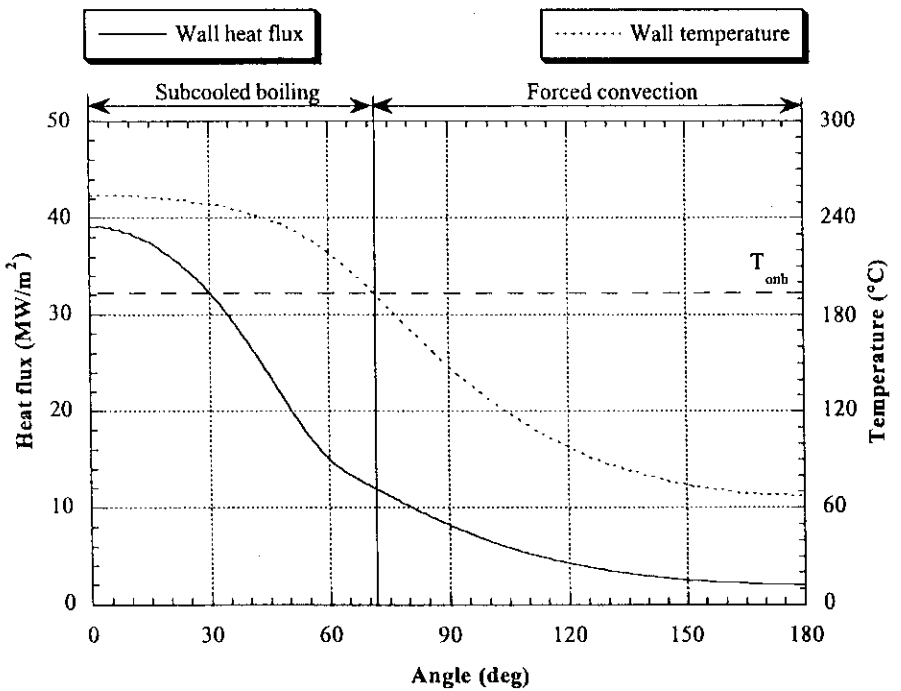

Fig. 17: Thermal hydraulic conditions and heat transfer analysis of test E44

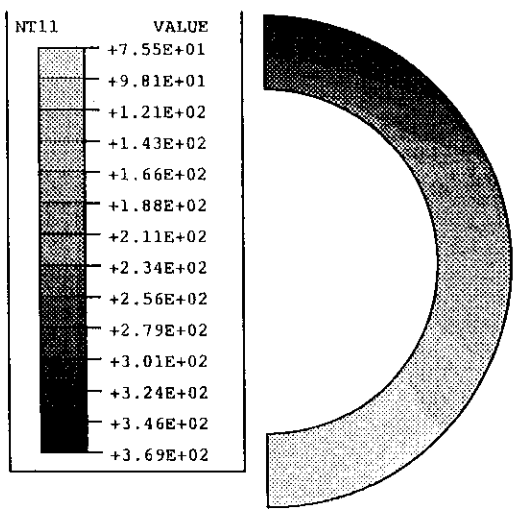

Isotherms in the material

Geometry and transversal incident flux profile	Longitudinal incident flux profile	L_h (mm)	P_{in} (MPa)	P_{out} (MPa)	P_{local} (MPa)	T_{in} (°C)	T_{out} (°C)	T_{local} (°C)	T_{sat}-T_{local} (°C)	G ($Mg.m^{-2}.s^{-1}$)	V_{axial} (m/s)	ΔP_{lineic} (MPa/m)	ICHF (MW/m^2)	Eng. WCHF (MW/m^2)	FE WCHF (MW/m^2)	FE peaking factor	Shot number
1996 **JAERI** OFHC-Cu OD = 10 mm ID = 7 mm PBEF Ion Beam Eng. Peaking factor: 1.43	1 0.3 0 $L_h/2$ L_h	160	1.2	1.0	1.0	29	47	38	141	12.0	12	0.29	25.3	36.1	32.2	1.27	E41

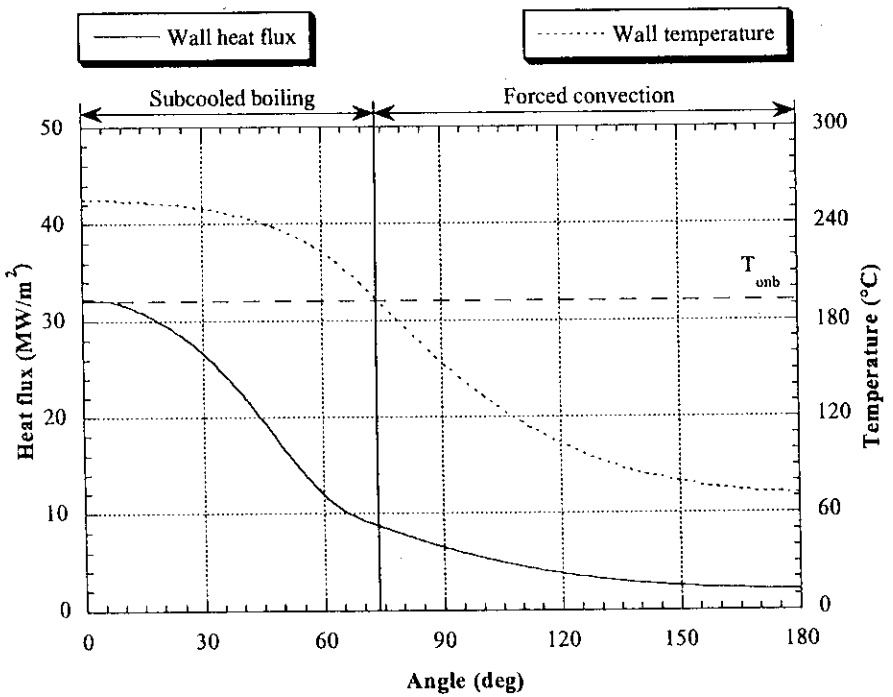

Fig. 18: Thermal hydraulic conditions and heat transfer analysis of test E41

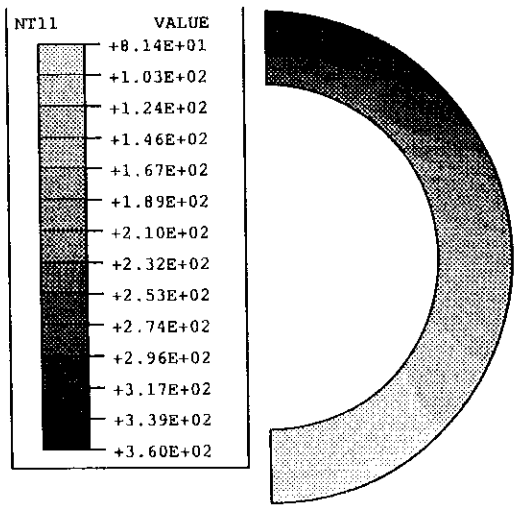

Isotherms in the material

Geometry and transversal incident flux profile	Longitudinal incident flux profile	L_h (mm)	P_{in} (MPa)	P_{out} (MPa)	P_{local} (MPa)	T_{in} (°C)	T_{out} (°C)	T_{local} (°C)	T_{sat}-T_{local} (°C)	G ($Mg.m^{-2}.s^{-1}$)	V_{axial} (m/s)	ΔP_{lineic} (MPa/m)	ICHF (MW/m^2)	Eng. WCHF (MW/m^2)	FE WCHF (MW/m^2)	FE peaking factor	Shot number
1996 **JAERI** OFHC-Cu OD = 10 mm ID = 7 mm PBEF Ion Beam Eng. Peaking factor: 1.43	1 0.3 0 $L_h/2$ L_h	160	1.2	1.0	1.0	28	47	38	141	10.0	10	0.18	21.8	31.1	27.5	1.26	E23

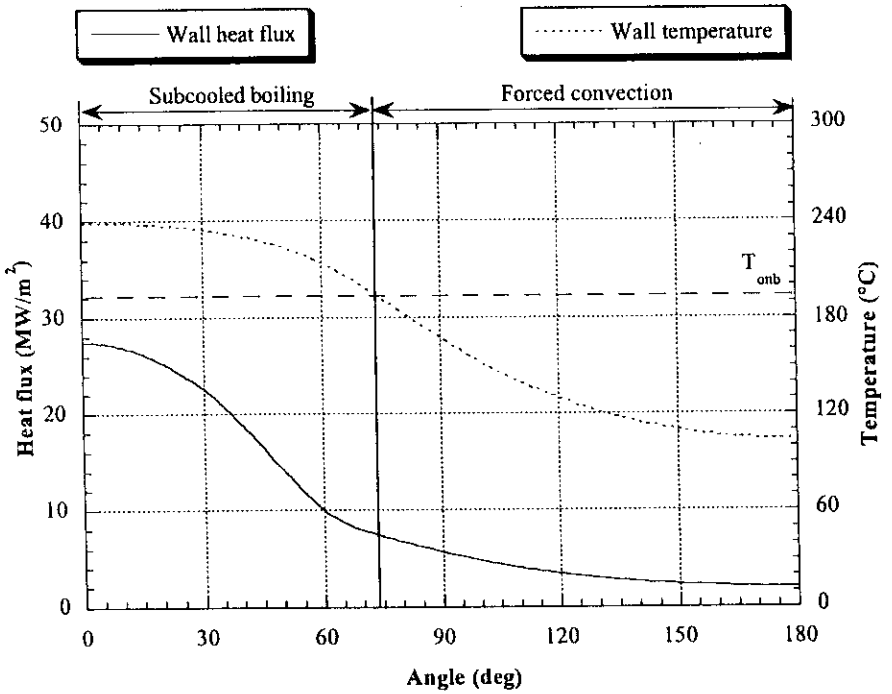

Fig. 19: Thermal hydraulic conditions and heat transfer analysis of test E23

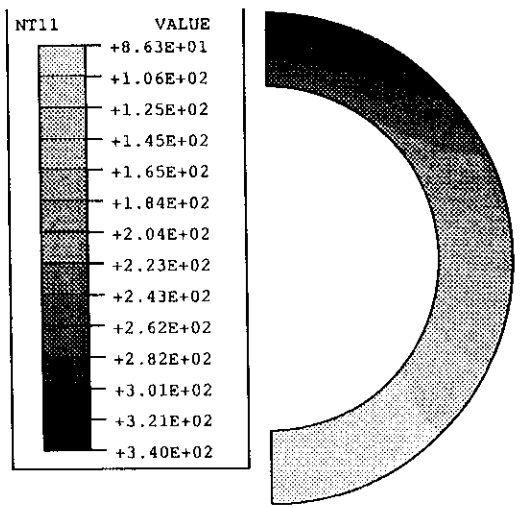

Isotherms in the material

Geometry and transversal incident flux profile	Longitudinal incident flux profile	L_h (mm)	P_{in} (MPa)	P_{out} (MPa)	P_{local} (MPa)	T_{in} (°C)	T_{out} (°C)	T_{local} (°C)	T_{sat}-T_{local} (°C)	G ($Mg.m^{-2}.s^{-1}$)	V_{axial} (m/s)	ΔP_{lineic} (MPa/m)	ICHF (MW/m^2)	Eng. WCHF (MW/m^2)	FE WCHF (MW/m^2)	FE peaking factor	Shot number
1996 **JAERI** OFHC-Cu OD = 10 mm ID = 7 mm PBEF Ion Beam Eng. Peaking factor: 1.43	1 0.3 0 $L_h/2$ L_h	160	1.2	1.0	1.0	28	51	40	139	8.1	8	0.13	21.8	31.1	27.6	1.27	E29

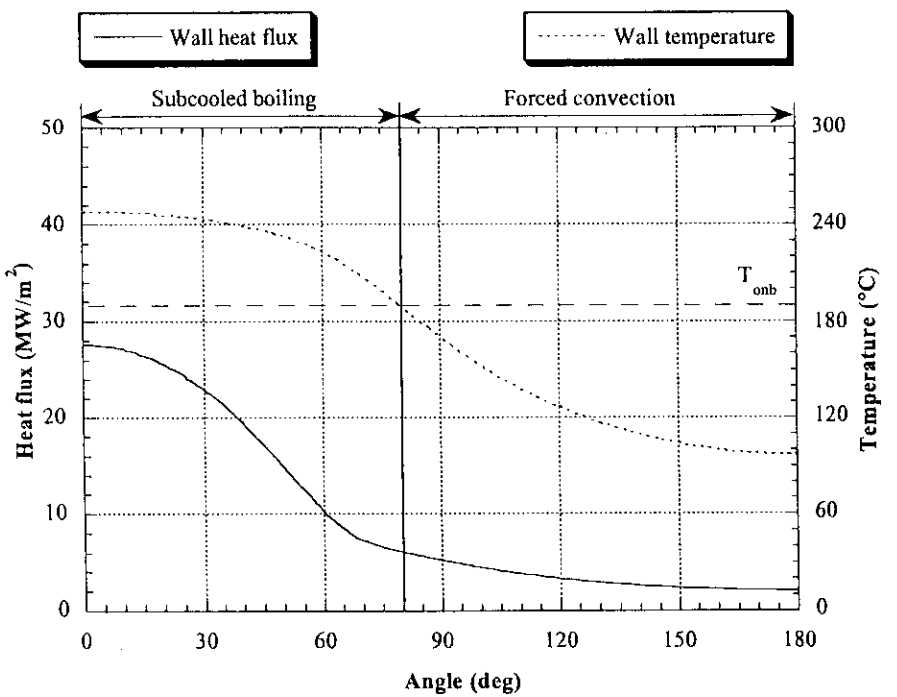

Fig. 20: Thermal hydraulic conditions and heat transfer analysis of test E29

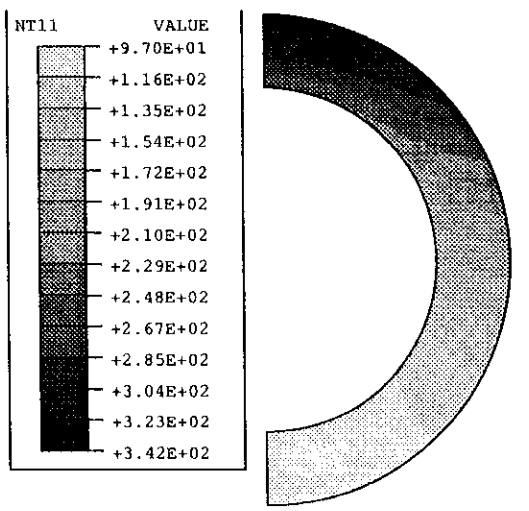

Isotherms in the material

Geometry and transversal incident flux profile	Longitudinal incident flux profile	L_h (mm)	P_{in} (MPa)	P_{out} (MPa)	P_{local} (MPa)	T_{in} (°C)	T_{out} (°C)	T_{local} (°C)	$T_{sat}-T_{local}$ (°C)	G ($Mg.m^{-2}.s^{-1}$)	V_{axial} (m/s)	ΔP_{lineic} (MPa/m)	ICHF (MW/m^2)	Eng. WCHF (MW/m^2)	FE WCHF (MW/m^2)	FE peaking factor	Shot number
1996 **JAERI** OFHC-Cu OD = 10 mm ID = 7 mm PBEF Ion Beam Eng. Peaking factor: 1.43	1 0.3 0 $L_h/2$ L_h	160	1.1	1.0	1.0	28	50	39	140	6.0	6	0.07	15.3	21.9	19.1	1.25	E30

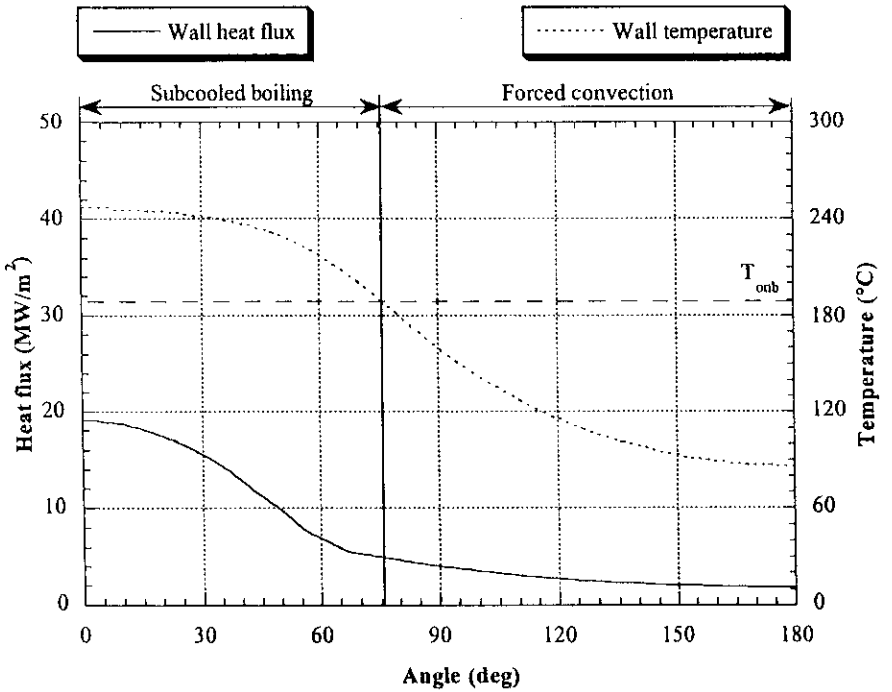

Fig. 21: Thermal hydraulic conditions and heat transfer analysis of test E30

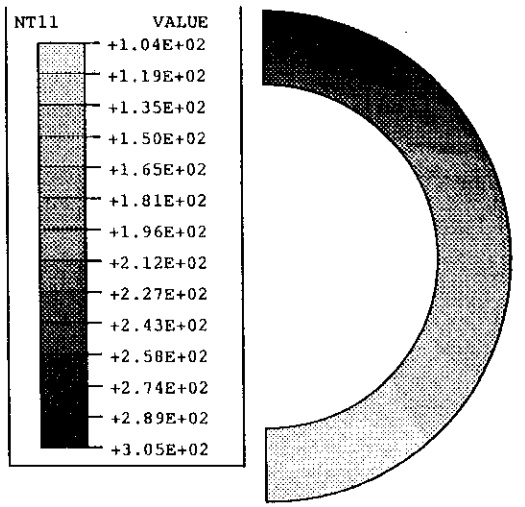

Isotherms in the material

Geometry and transversal incident flux profile	Longitudinal incident flux profile	L_h (mm)	P_{in} (MPa)	P_{out} (MPa)	P_{local} (MPa)	T_{in} (°C)	T_{out} (°C)	T_{local} (°C)	T_{sat}-T_{local} (°C)	G ($Mg.m^{-2}.s^{-1}$)	V_{axial} (m/s)	$\Delta P_{linetic}$ (MPa/m)	ICHF (MW/m^2)	Eng. WCHF (MW/m^2)	FE WCHF (MW/m^2)	FE peaking factor	Shot number
1996 JAERI Material :OFHC-Cu OD = 10 mm ID = 7 mm Twist ratio:3 Tape thickness:0.35 mm Tape material: Inconel 625 PBEF Ion Beam Eng. Peaking factor: 1.43	1 0.3 0 $L_h/2$ L_h	160	1.7	1.3	1.5	24	61	43	155	14.0	14	0.90	39.6	56.6	52.3	1.32	B52

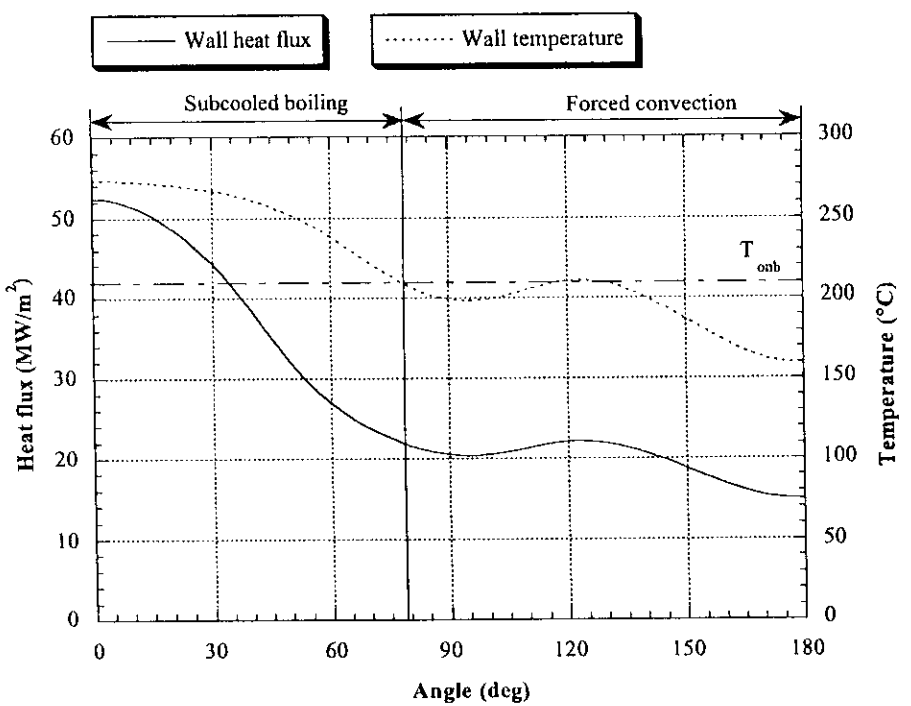

Fig. 22: Thermal hydraulic conditions and heat transfer analysis of test B52

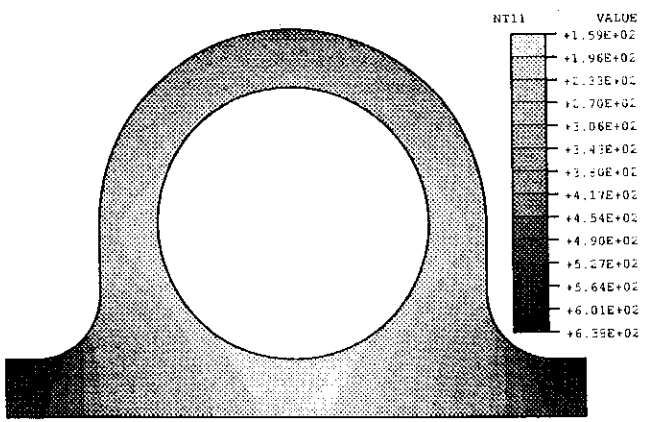

Isotherms in the material

Geometry and transversal incident flux profile	Longitudinal incident flux profile	L_h (mm)	P_{in} (MPa)	P_{out} (MPa)	P_{local} (MPa)	T_{in} (°C)	T_{out} (°C)	T_{local} (°C)	$T_{sat}-T_{local}$ (°C)	G ($Mg.m^{-2}.s^{-1}$)	V_{axial} (m/s)	ΔP_{lineic} (MPa/m)	ICHF (MW/m^2)	Eng. WCHF (MW/m^2)	FE WCHF (MW/m^2)	FE peaking factor	Shot number
1996 JAERI Material :OFHC-Cu OD = 10 mm ID = 7 mm Twist ratio:3 Tape thickness:0.35 mm Tape material: Inconel 625 PBEF Ion Beam Eng. Peaking factor: 1.43	1, 0.3, 0, $L_h/2$, L_h	160	1.7	1.4	1.5	25	64	45	153	12.0	12	0.68	36.8	52.6	49.1	1.33	B47

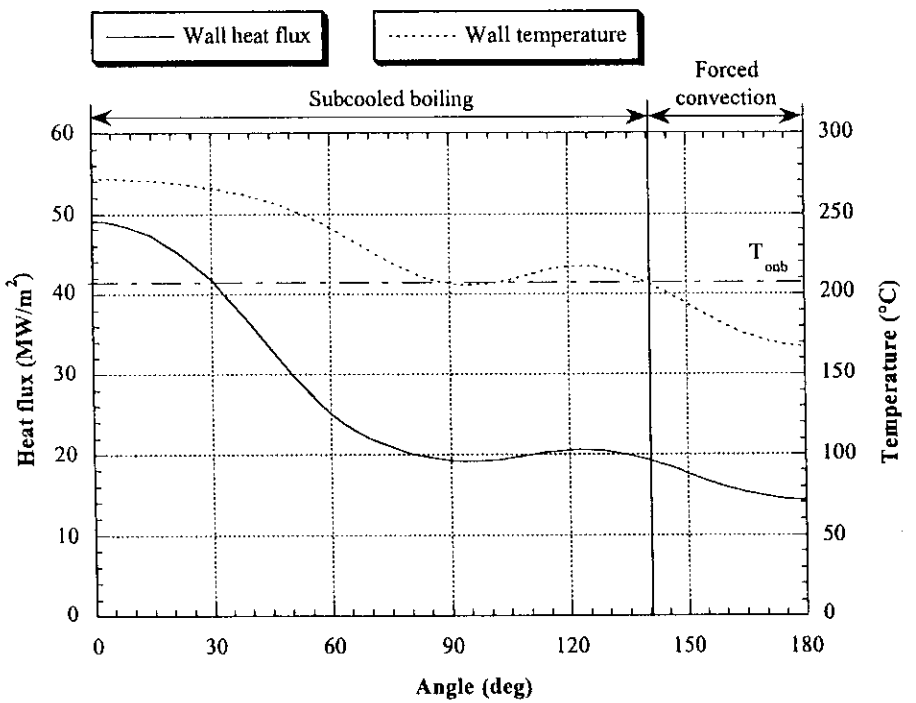

Fig. 23: Thermal hydraulic conditions and heat transfer analysis of test B47

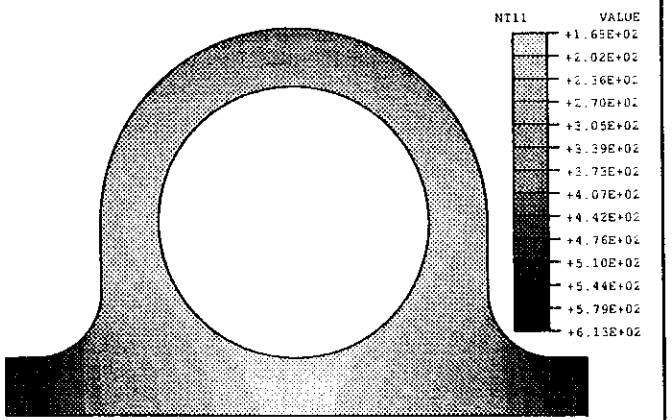

Isotherms in the material

Geometry and transversal incident flux profile	Longitudinal incident flux profile	L_h (mm)	P_{in} (MPa)	P_{out} (MPa)	P_{local} (MPa)	T_{in} (°C)	T_{out} (°C)	T_{local} (°C)	T_{sat}-T_{local} (°C)	G ($Mg.m^{-2}.s^{-1}$)	V_{axial} (m/s)	ΔP_{lineic} (MPa/m)	ICHF (MW/m^2)	Eng. WCHF (MW/m^2)	FE WCHF (MW/m^2)	FE peaking factor	Shot number
1996 **JAERI** Material :OFHC-Cu OD = 10 mm ID = 7 mm Twist ratio:3 Tape thickness:0.35 mm Tape material: Inconel 625 PBEF Ion Beam Eng. Peaking factor: 1.43	1 0.3 0 $L_h/2$ L_h	160	1.6	1.4	1.5	25	70	48	150	10.0	10	0.47	34.7	49.6	46.9	1.35	B30

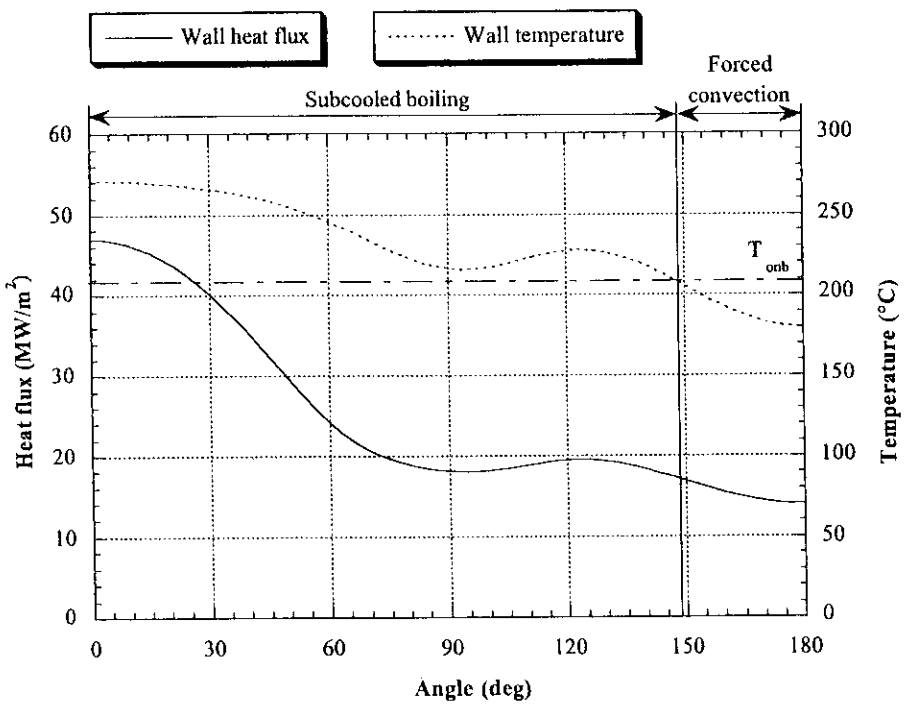

Fig. 24: Thermal hydraulic conditions and heat transfer analysis of B30

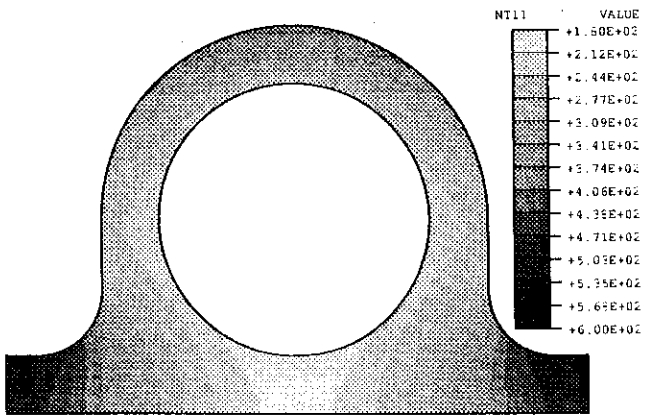

Isotherms in the material

Geometry and transversal incident flux profile	Longitudinal incident flux profile	L_h (mm)	P_{in} (MPa)	P_{out} (MPa)	P_{local} (MPa)	T_{in} (°C)	T_{out} (°C)	T_{local} (°C)	T_{sat}-T_{local} (°C)	G ($Mg.m^{-2}.s^{-1}$)	V_{axial} (m/s)	ΔP_{lineic} (MPa/m)	ICHF (MW/m^2)	Eng. WCHF (MW/m^2)	FE WCHF (MW/m^2)	FE peaking factor	Shot number
1996 **JAERI** Material :OFHC-Cu OD = 10 mm ID = 7 mm Twist ratio:3 Tape thickness:0.35 mm Tape material: Inconel 625 PBEF Ion Beam Eng. Peaking factor: 1.43	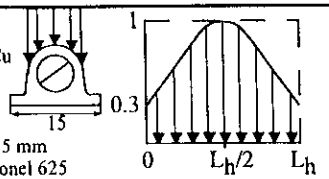	160	1.6	1.4	1.5	25	75	50	148	8.0	8	0.30	30.7	43.9	42.0	1.37	B36

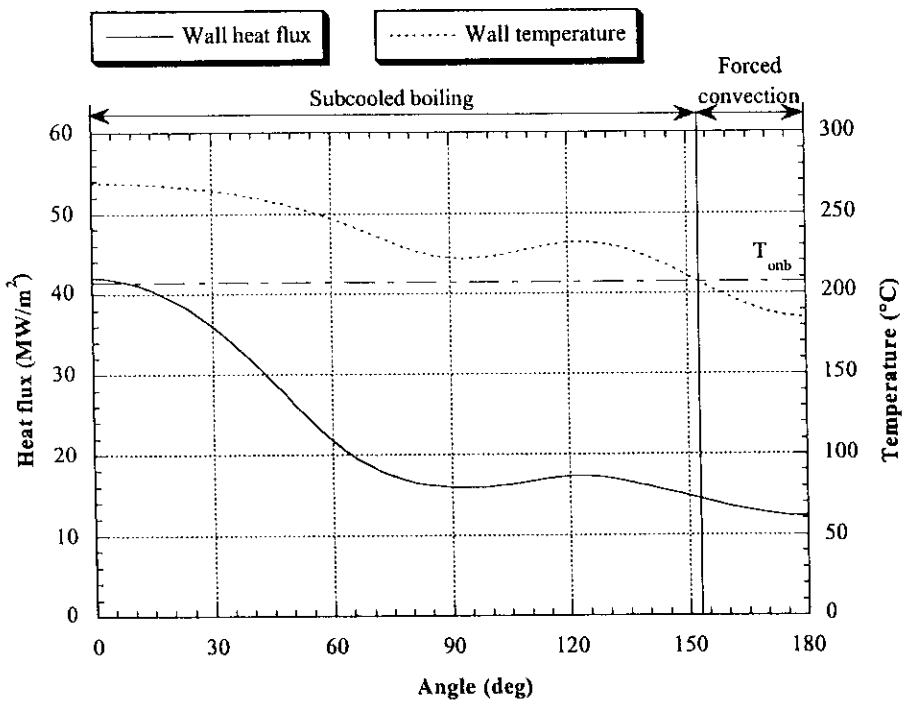

Fig. 25: Thermal hydraulic conditions and heat transfer analysis of B36

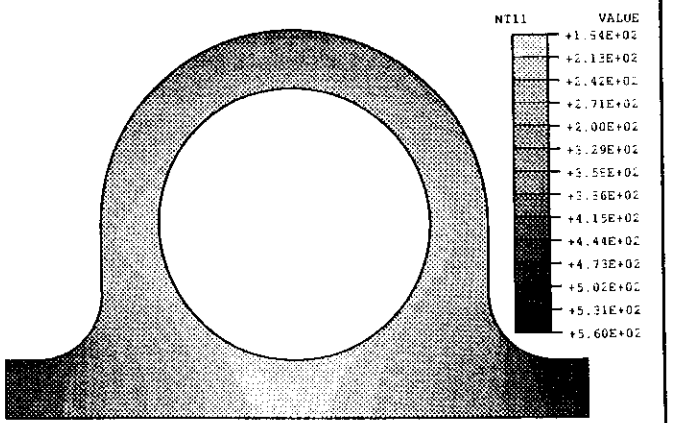

Isotherms in the material

Geometry and transversal incident flux profile	Longitudinal incident flux profile	L_h (mm)	P_{in} (MPa)	P_{out} (MPa)	P_{local} (MPa)	T_{in} (°C)	T_{out} (°C)	T_{local} (°C)	$T_{sat}-T_{local}$ (°C)	G ($Mg.m^{-2}.s^{-1}$)	V_{axial} (m/s)	ΔP_{lineic} (MPa/m)	ICHF (MW/m^2)	Eng. WCHF (MW/m^2)	FE WCHF (MW/m^2)	FE peaking factor	Shot number
1996 **JAERI** Material :OFHC-Cu OD = 10 mm ID = 7 mm Twist ratio:3 Tape thickness:0.35 mm Tape material: Inconel 625 PBEF Ion Beam Eng. Peaking factor: 1.43	1 0.3 0 $L_h/2$ L_h	160	1.6	1.5	1.5	25	83	54	144	6.0	6	0.17	27.0	38.6	37.7	1.40	B39

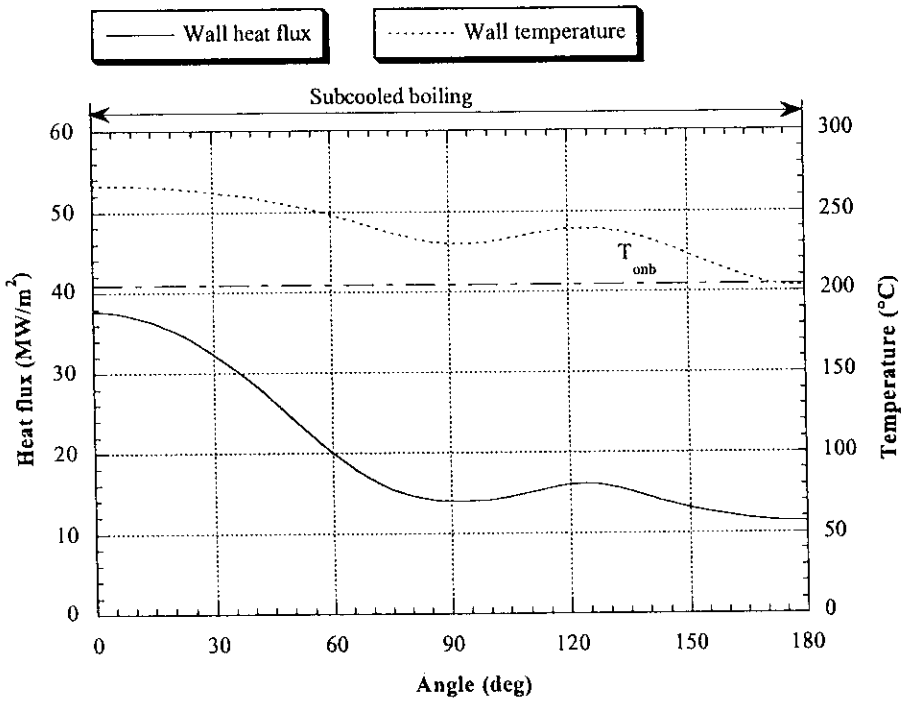

Fig. 26: Thermal hydraulic conditions and heat transfer analysis of B39

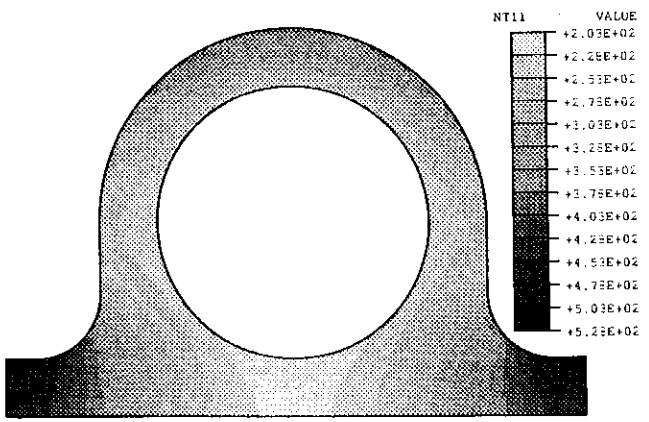

Isotherms in the material

Geometry and transversal incident flux profile	Longitudinal incident flux profile	L_h (mm)	P_{in} (MPa)	P_{out} (MPa)	P_{local} (MPa)	T_{in} (°C)	T_{out} (°C)	T_{local} (°C)	T_{sat}-T_{local} (°C)	G ($Mg.m^{-2}.s^{-1}$)	V_{axial} (m/s)	ΔP_{lineic} (MPa/m)	ICHF (MW/m^2)	Eng. WCHF (MW/m^2)	FE WCHF (MW/m^2)	FE peaking factor	Shot number
1996 **JAERI** Material :OFHC-Cu OD = 10 mm ID = 7 mm Twist ratio:3 Tape thickness:0.35 mm Tape material: Inconel 625 PBEF Ion Beam Eng. Peaking factor: 1.43	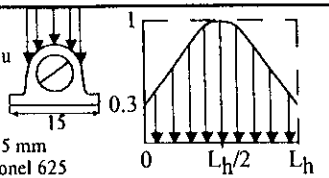	160	1.6	1.5	1.5	24	87	56	142	4.1	4	0.09	19.8	28.3	27.8	1.40	B42

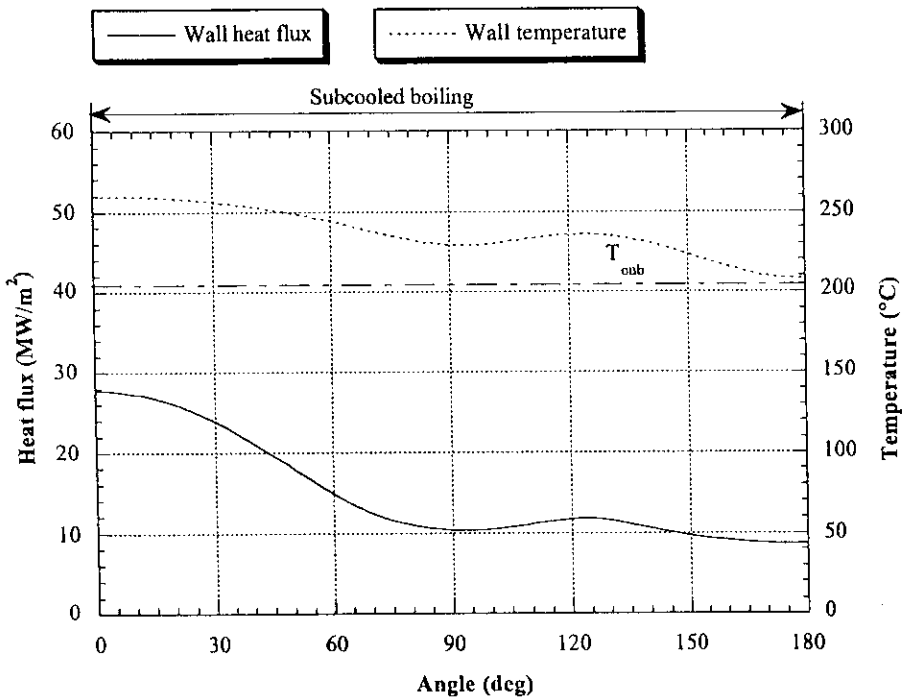

Fig. 27: Thermal hydraulic conditions and heat transfer analysis of B42

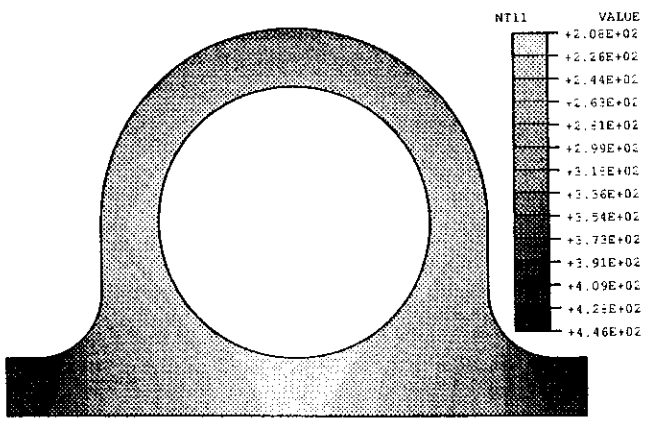

Isotherms in the material

Geometry and transversal incident flux profile	Longitudinal incident flux profile	L_h (mm)	P_{in} (MPa)	P_{out} (MPa)	P_{local} (MPa)	T_{in} (°C)	T_{out} (°C)	T_{local} (°C)	$T_{sat}-T_{local}$ (°C)	G ($Mg.m^{-2}.s^{-1}$)	V_{axial} (m/s)	ΔP_{linear} (MPa/m)	ICHF (MW/m^2)	Eng. WCHF (MW/m^2)	FE WCHF (MW/m^2)	FE peaking factor	Shot number
1996 **JAERI** Material :OFHC-Cu OD = 10 mm ID = 7 mm Twist ratio:3 Tape thickness:0.35 mm Tape material: Inconel 625 PBEF Ion Beam Eng. Peaking factor: 1.43	1 0.3 0 $L_h/2$ L_h	160	1.4	0.6	1.0	22	51	37	142	20.0	20	1.82	45.8	65.4	59.1	1.29	C35

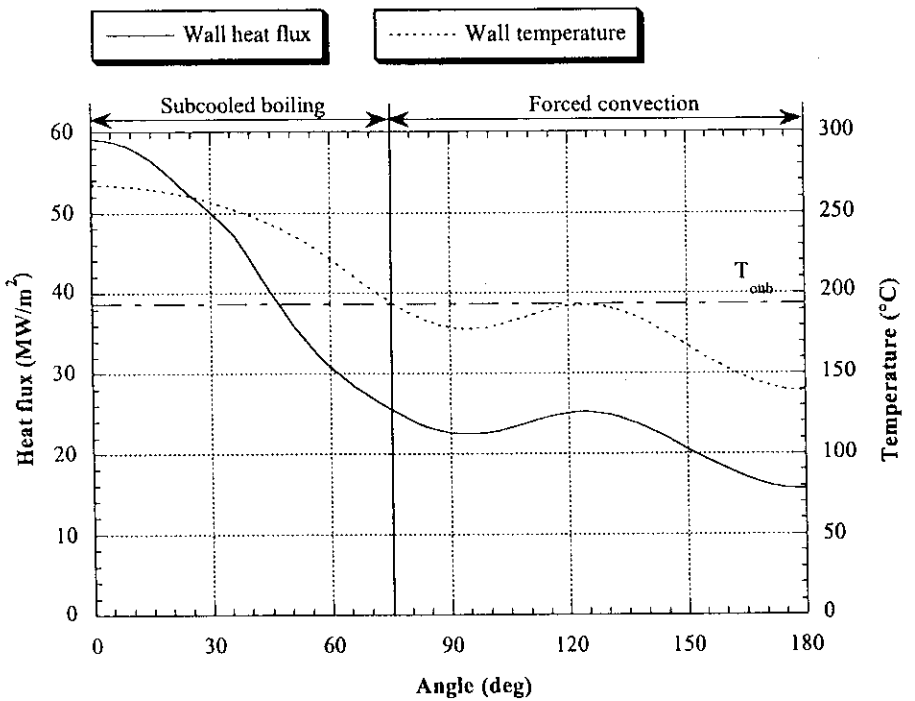

Fig. 28: Thermal hydraulic conditions and heat transfer analysis of C35

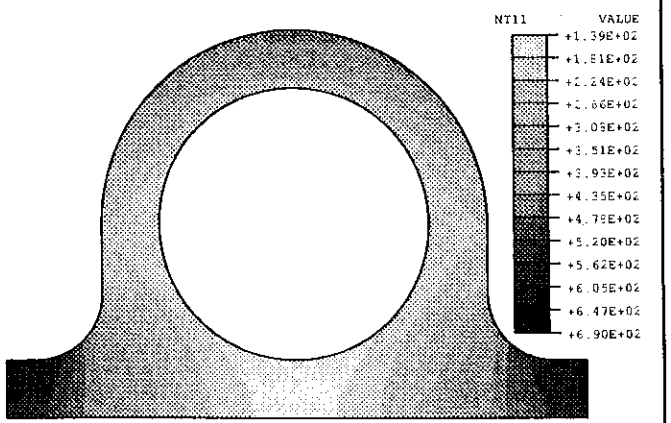

Isotherms in the material

Geometry and transversal incident flux profile	Longitudinal incident flux profile	L_h (mm)	P_{in} (MPa)	P_{out} (MPa)	P_{local} (MPa)	T_{in} (°C)	T_{out} (°C)	T_{local} (°C)	T_{sat}-T_{local} (°C)	G ($Mg.m^{-2}.s^{-1}$)	V_{axial} (m/s)	ΔP_{lineic} (MPa/m)	ICHF (MW/m^2)	Eng. WCHF (MW/m^2)	FE WCHF (MW/m^2)	FE peaking factor	Shot number
1996 JAERI Material :OFHC-Cu OD = 10 mm ID = 7 mm Twist ratio:3 Tape thickness:0.35 mm Tape material: Inconel 625 PBEF Ion Beam Eng. Peaking factor: 1.43	1, 0.3, 0, $L_h/2$, L_h	160	1.3	0.7	1.0	21	52	37	142	18.0	18	1.49	43.5	62.1	58.4	1.34	C30

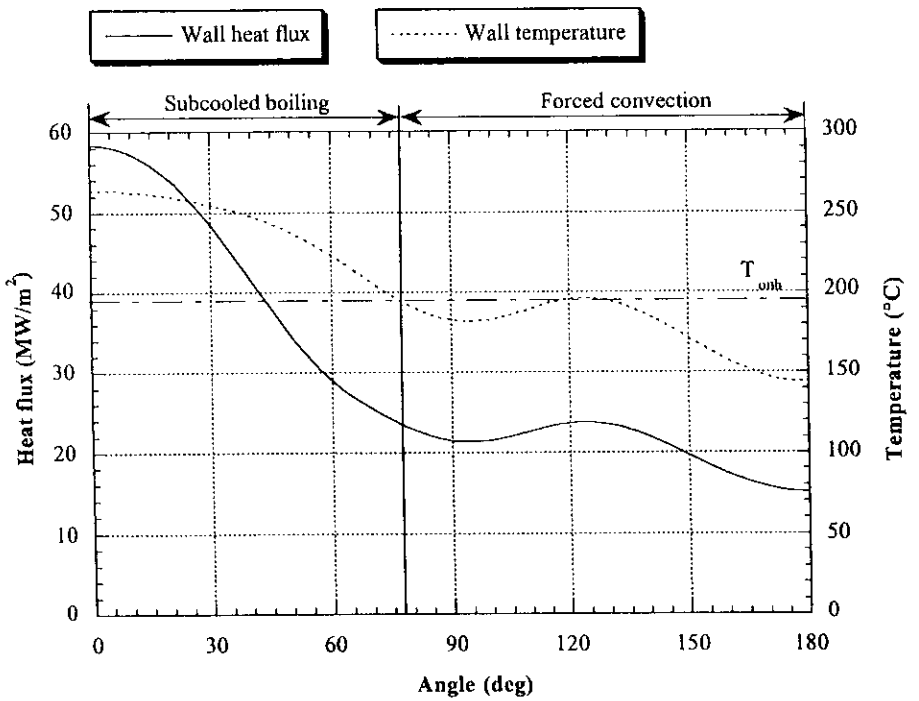

Fig. 29: Thermal hydraulic conditions and heat transfer analysis of C30

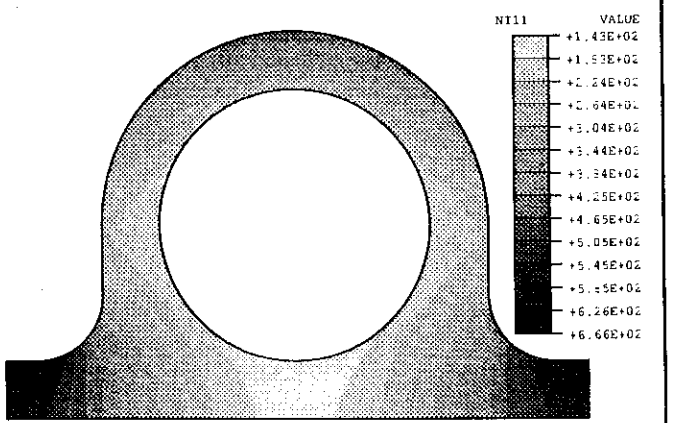

Isotherms in the material

Geometry and transversal incident flux profile	Longitudinal incident flux profile	L_h (mm)	P_{in} (MPa)	P_{out} (MPa)	P_{local} (MPa)	T_{in} (°C)	T_{out} (°C)	T_{local} (°C)	T_{sat}-T_{local} (°C)	G ($Mg.m^{-2}.s^{-1}$)	V_{axial} (m/s)	ΔP_{lineic} (MPa/m)	ICHF (MW/m^2)	Eng. WCHF (MW/m^2)	FE WCHF (MW/m^2)	FE peaking factor	Shot number
1996 **JAERI** Material :OFHC-Cu OD = 10 mm ID = 7 mm Twist ratio:3 Tape thickness:0.35 mm Tape material: Inconel 625 PBEF Ion Beam Eng. Peaking factor: 1.43	1 0.3 0 $L_h/2$ L_h	160	1.3	0.8	1.0	21	55	38	141	16.0	16	1.19	41.6	59.4	54.0	1.30	C25

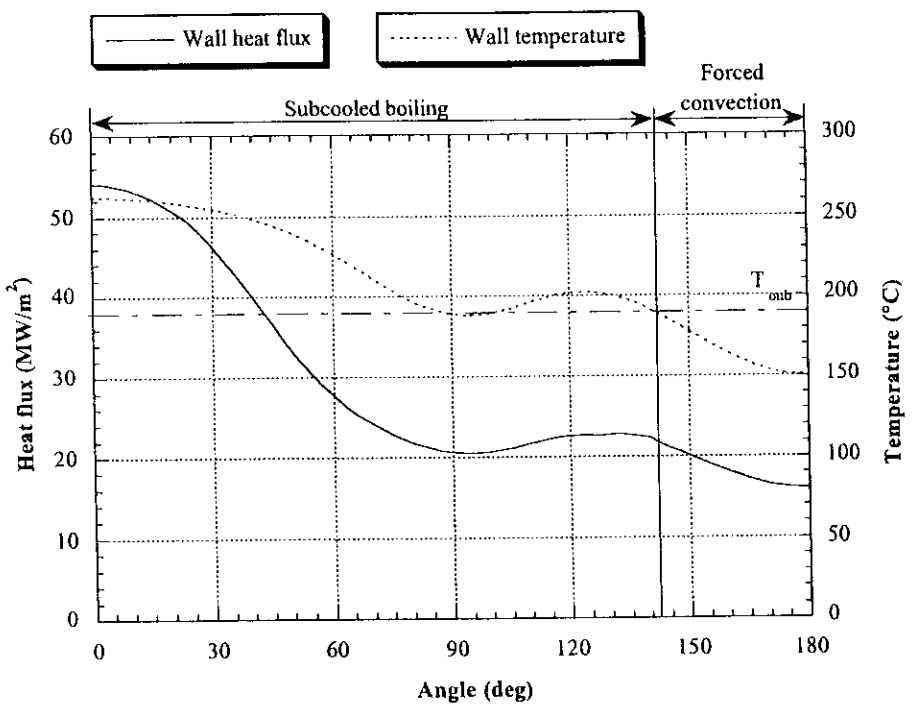

Fig. 30: Thermal hydraulic conditions and heat transfer analysis of C25

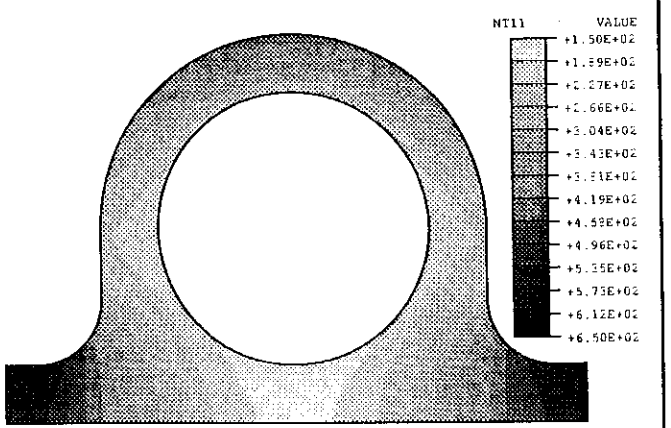

Isotherms in the material

Geometry and transversal incident flux profile	Longitudinal incident flux profile	L_h (mm)	P_{in} (MPa)	P_{out} (MPa)	P_{local} (MPa)	T_{in} (°C)	T_{out} (°C)	T_{local} (°C)	T_{sat}-T_{local} (°C)	G ($Mg.m^{-2}.s^{-1}$)	V_{axial} (m/s)	ΔP_{lineic} (MPa/m)	ICHF (MW/m^2)	Eng. WCHF (MW/m^2)	FE WCHF (MW/m^2)	FE peaking factor	Shot number
1996 **JAERI** Material :OFHC-Cu OD = 10 mm ID = 7 mm Twist ratio:3 Tape thickness:0.35 mm Tape material: Inconel 625 PBEF Ion Beam Eng. Peaking factor: 1.43	1 0.3 0 $L_h/2$ L_h	160	1.3	0.8	1.0	21	58	40	139	14.1	14	0.93	39.6	56.6	52.6	1.33	C20

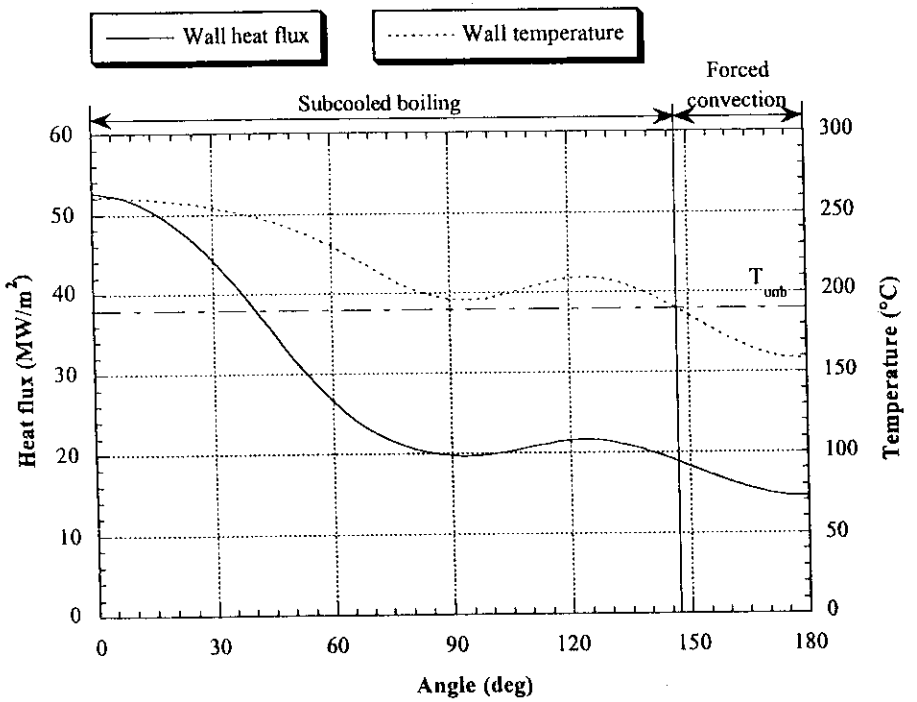

Fig. 31: Thermal hydraulic conditions and heat transfer analysis of C20

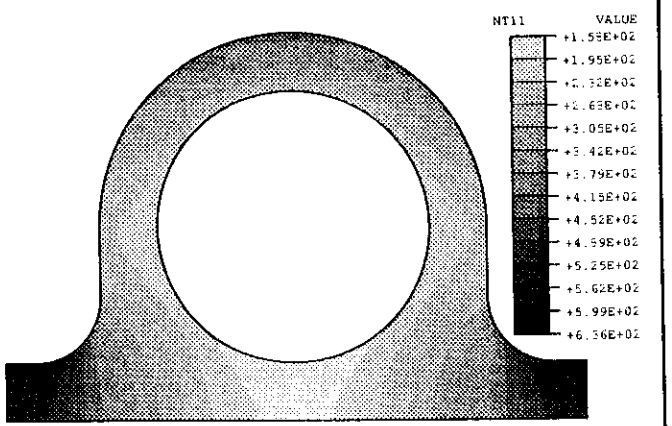

Isotherms in the material

Geometry and transversal incident flux profile	Longitudinal incident flux profile	L_h (mm)	P_{in} (MPa)	P_{out} (MPa)	P_{local} (MPa)	T_{in} (°C)	T_{out} (°C)	T_{local} (°C)	T_{sat}-T_{local} (°C)	G ($Mg.m^{-2}.s^{-1}$)	V_{axial} (m/s)	ΔP_{lineic} (MPa/m)	ICHF (MW/m^2)	Eng. WCHF (MW/m^2)	FE WCHF (MW/m^2)	FE peaking factor	Shot number
1996 **JAERI** Material :OFHC-Cu OD = 10 mm ID = 7 mm Twist ratio:3 Tape thickness:0.35 mm Tape material: Inconel 625 PBEF Ion Beam Eng. Peaking factor: 1.43	1 0.3 0 $L_h/2$ L_h	160	1.2	0.9	1.0	22	61	41	138	12.1	12	0.71	36.8	52.6	48.5	1.32	C15

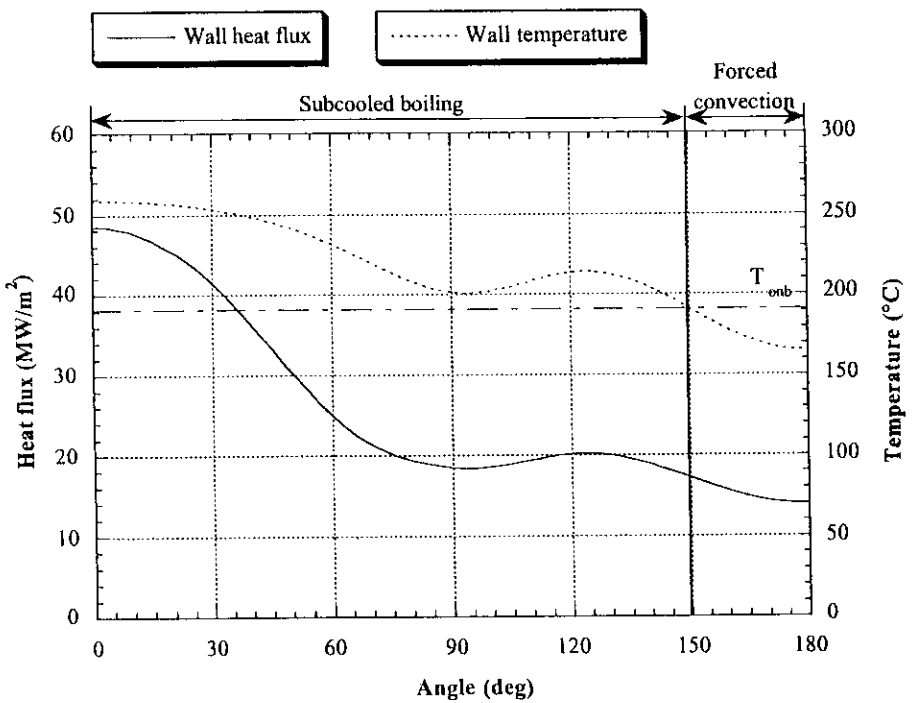

Fig. 32: Thermal hydraulic conditions and heat transfer analysis of C15

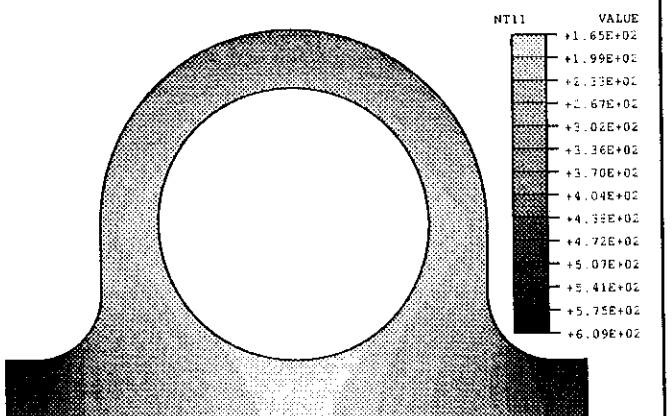

Isotherms in the material

Geometry and transversal incident flux profile	Longitudinal incident flux profile	L_h (mm)	P_{in} (MPa)	P_{out} (MPa)	P_{local} (MPa)	T_{in} (°C)	T_{out} (°C)	T_{local} (°C)	T_{sat}-T_{local} (°C)	G ($Mg.m^{-2}.s^{-1}$)	V_{axial} (m/s)	ΔP_{lineic} (MPa/m)	ICHF (MW/m^2)	Eng. WCHF (MW/m^2)	FE WCHF (MW/m^2)	FE peaking factor	Shot number
1996 **JAERI** Material :OFHC-Cu OD = 10 mm ID = 7 mm Twist ratio:3 Tape thickness:0.35 mm Tape material: Inconel 625 PBEF Ion Beam Eng. Peaking factor: 1.43	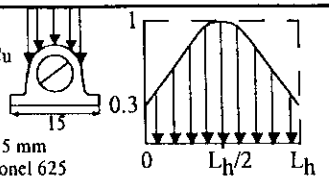	160	1.2	0.9	1.0	23	65	45	135	10.0	10	0.48	34.7	49.6	46.6	1.34	B57

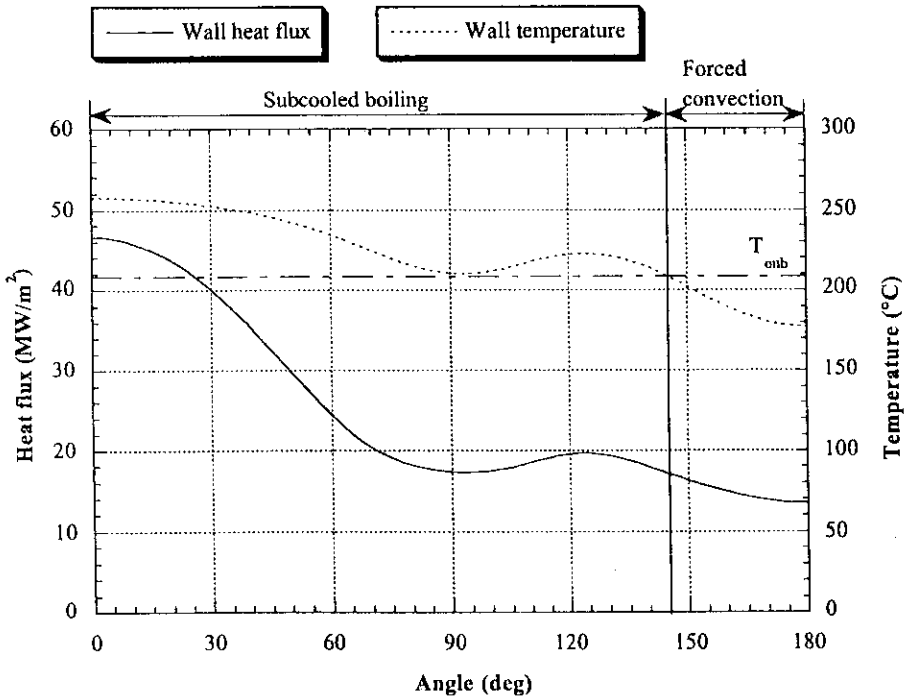

Fig. 33: Thermal hydraulic conditions and heat transfer analysis of B57

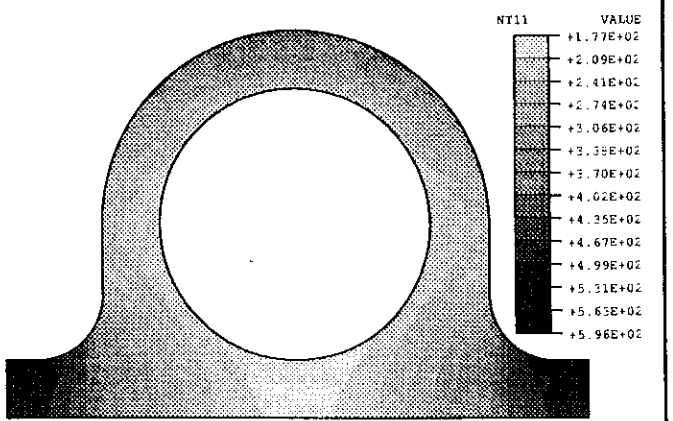

Isotherms in the material

Geometry and transversal incident flux profile	Longitudinal incident flux profile	L_h (mm)	P_{in} (MPa)	P_{out} (MPa)	P_{local} (MPa)	T_{in} (°C)	T_{out} (°C)	T_{local} (°C)	T_{sat}-T_{local} (°C)	G ($Mg.m^{-2}.s^{-1}$)	V_{axial} (m/s)	ΔP_{lineic} (MPa/m)	ICHF (MW/m^2)	Eng. WCHF (MW/m^2)	FE WCHF (MW/m^2)	FE peaking factor	Shot number
1996 JAERI Material :OFHC-Cu OD = 10 mm ID = 7 mm Twist ratio:3 Tape thickness:0.35 mm Tape material: Inconel 625 PBEF Ion Beam Eng. Peaking factor: 1.43	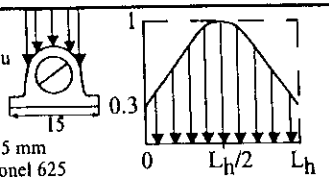	160	1.1	0.9	1.0	24	70	47	132	8.0	8	0.32	28.9	41.3	39.1	1.35	B60

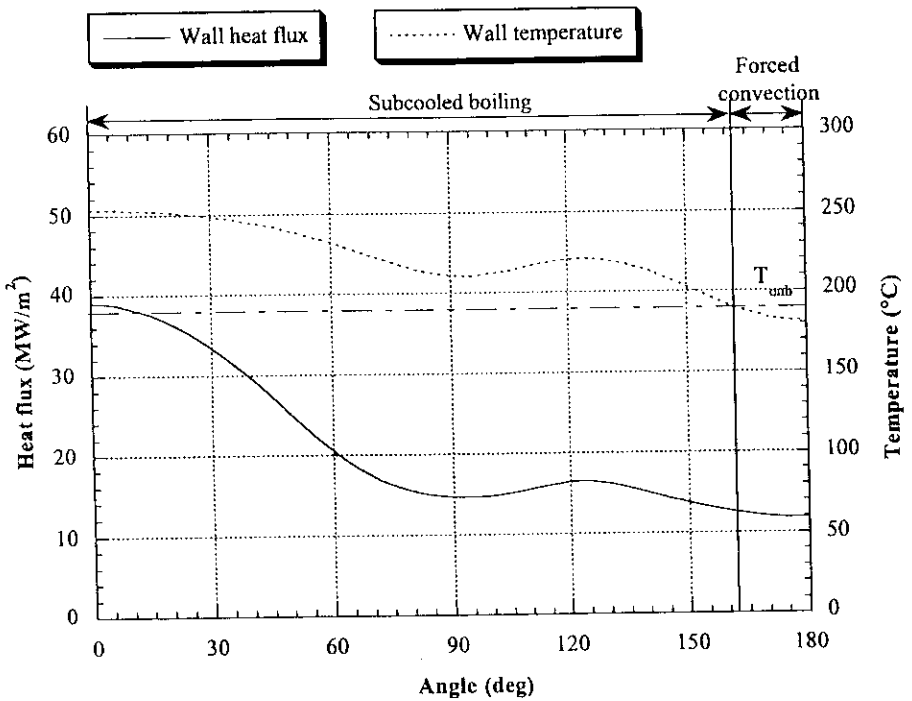

Fig. 34: Thermal hydraulic conditions and heat transfer analysis of B60

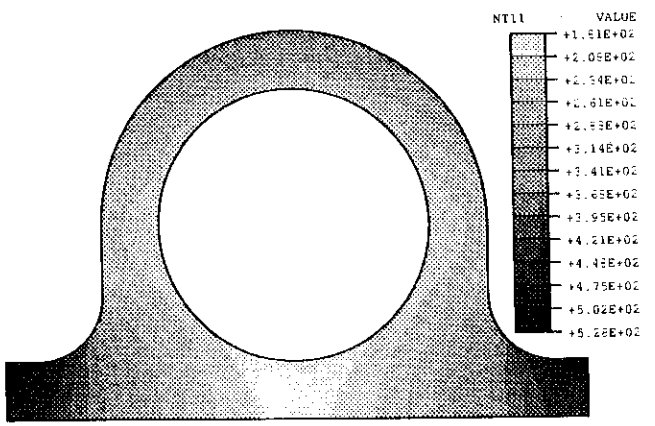

Isotherms in the material

Geometry and transversal incident flux profile	Longitudinal incident flux profile	L_h (mm)	P_{in} (MPa)	P_{out} (MPa)	P_{local} (MPa)	T_{in} (°C)	T_{out} (°C)	T_{local} (°C)	T_{sat}-T_{local} (°C)	G ($Mg.m^{-2}.s^{-1}$)	V_{axial} (m/s)	ΔP_{lineic} (MPa/m)	ICHF (MW/m^2)	Eng. WCHF (MW/m^2)	FE WCHF (MW/m^2)	FE peaking factor	Shot number
1996 **JAERI** Material :OFHC-Cu OD = 10 mm ID = 7 mm Twist ratio:3 Tape thickness:0.35 mm Tape material: Inconel 625 PBEF Ion Beam Eng. Peaking factor: 1.43	1 0.3 0 $L_h/2$ L_h	160	1.1	1.0	1.0	23	78	50	129	6.0	6	0.17	25.4	36.3	34.8	1.37	C05

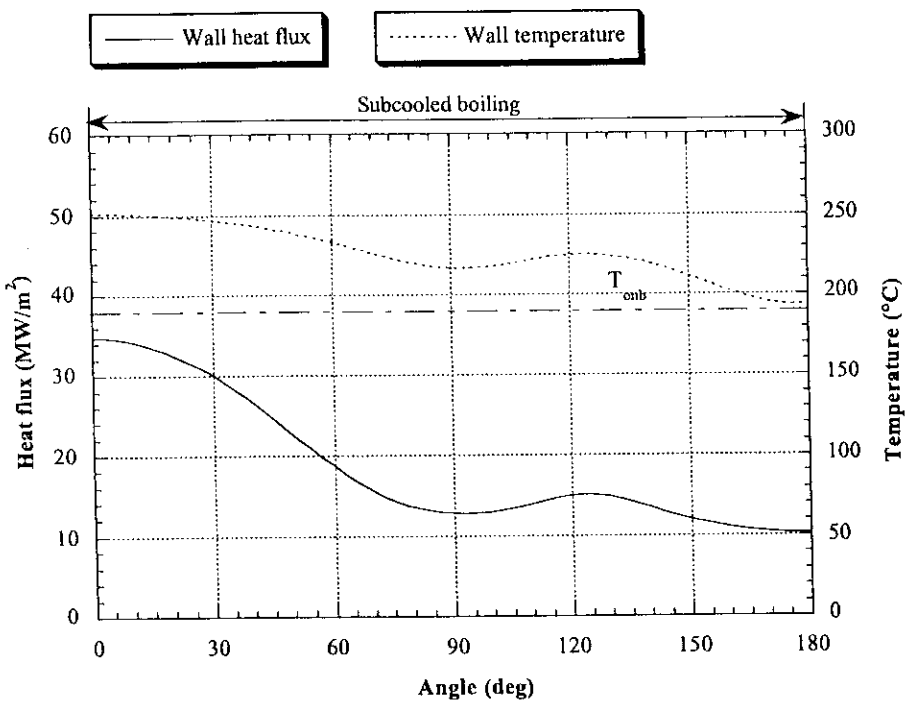

Fig. 35: Thermal hydraulic conditions and heat transfer analysis of C05

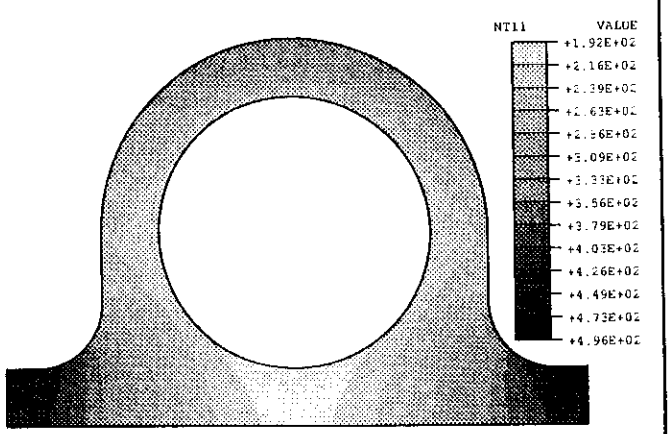

Isotherms in the material

Geometry and transversal incident flux profile	Longitudinal incident flux profile	L_h (mm)	P_{in} (MPa)	P_{out} (MPa)	P_{local} (MPa)	T_{in} (°C)	T_{out} (°C)	T_{local} (°C)	T_{sat}-T_{local} (°C)	G ($Mg.m^{-2}.s^{-1}$)	V_{axial} (m/s)	ΔP_{linear} (MPa/m)	ICHF (MW/m^2)	Eng. WCHF (MW/m^2)	FE WCHF (MW/m^2)	FE peaking factor	Shot number
1996 **JAERI** Material :OFHC-Cu OD = 10 mm ID = 7 mm Twist ratio:3 Tape thickness:0.35 mm Tape material: Inconel 625 PBEF Ion Beam Eng. Peaking factor: 1.43	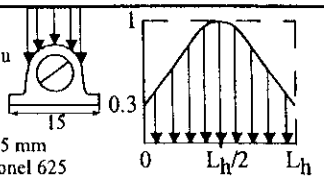	160	1.1	1.0	1.0	23	93	58	121	4.0	4	0.11	21.8	31.1	31.1	1.43	C10

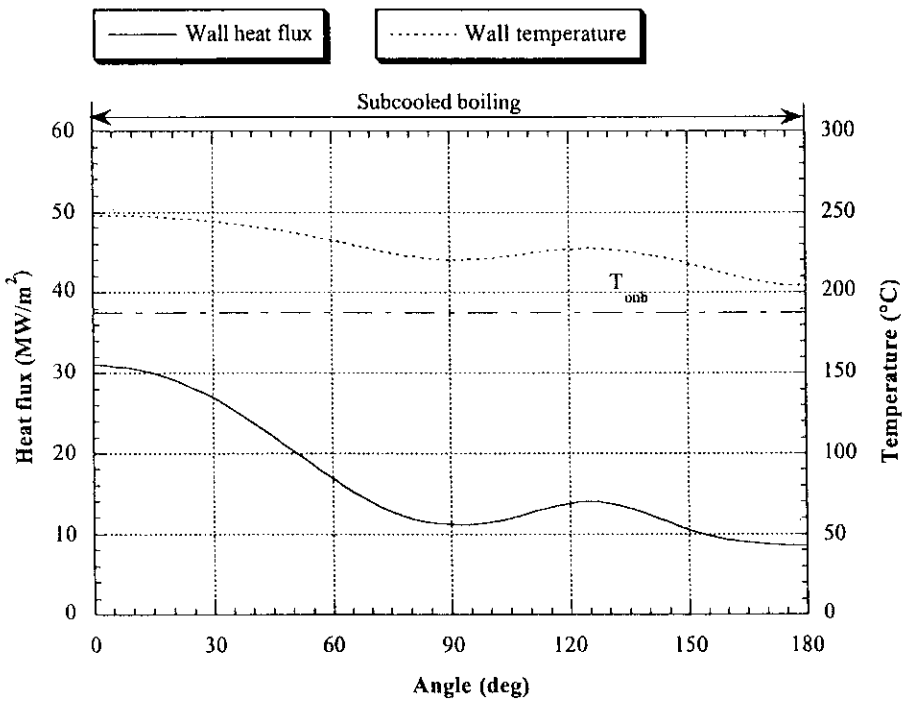

Fig. 36: Thermal hydraulic conditions and heat transfer analysis of C10

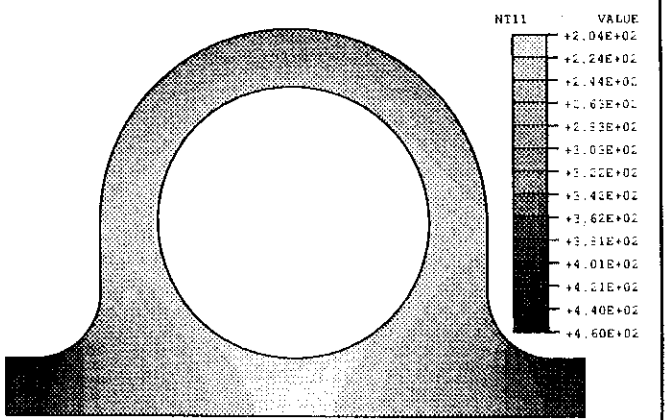

Isotherms in the material

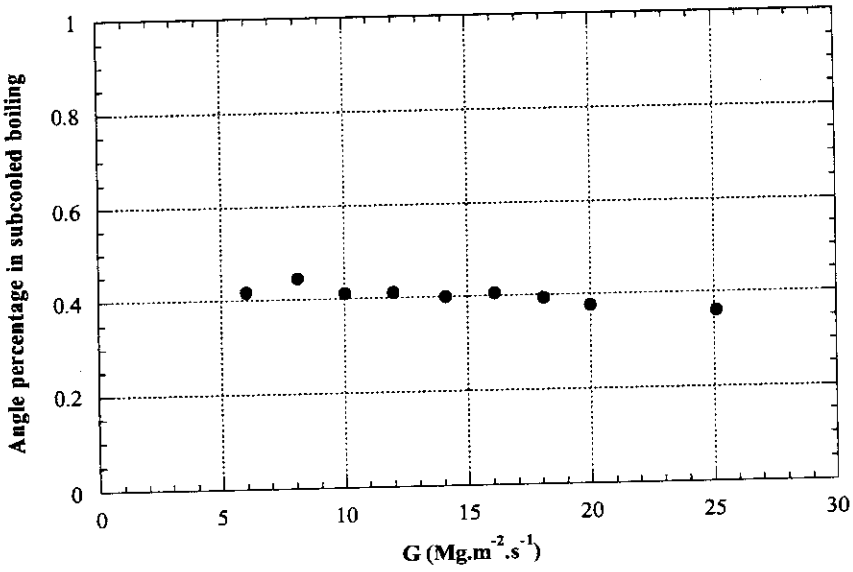

Fig. 37: Angle percentage in subcooled boiling of smooth tube

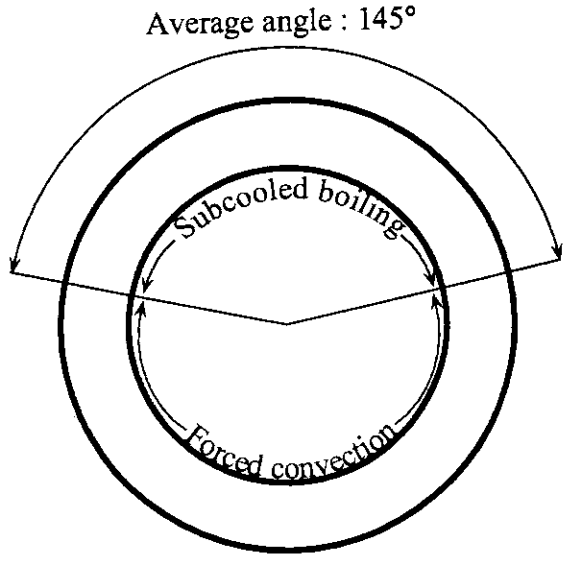

Fig. 38: Distribution of heat transfer regimes at the inner wall of smooth tube

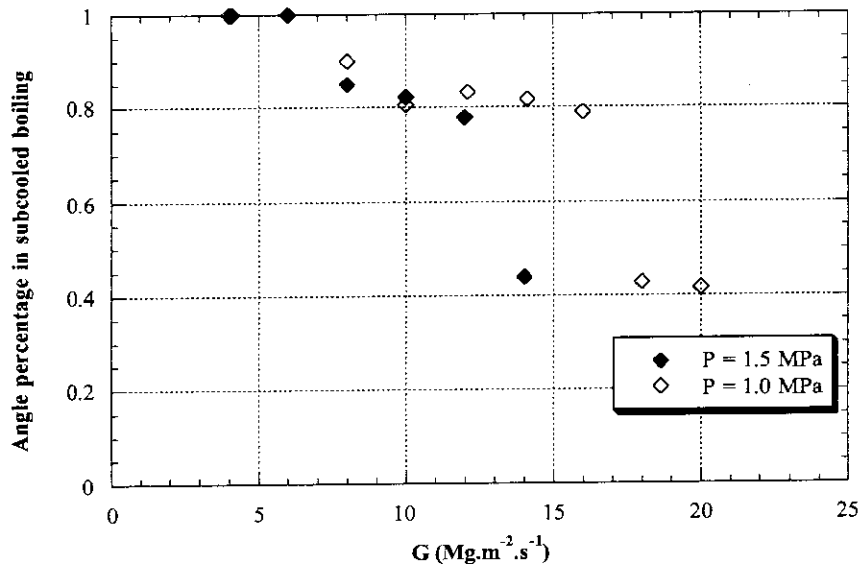

Fig. 39: Angle percentage in subcooled boiling of externally-finned swirl tube

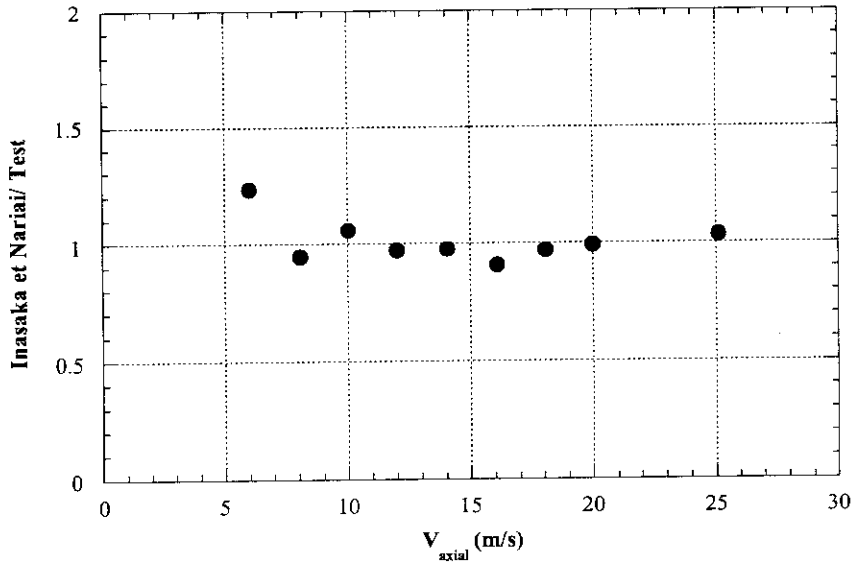

Figure 40: Comparison between test results and Inasaka et Nariai correlation for smooth tube

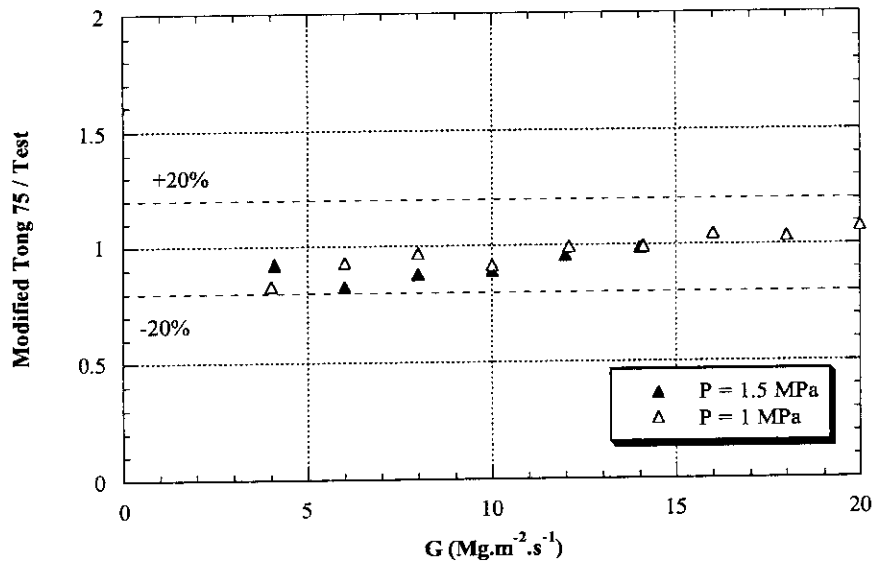

Figure 41: Comparison between test results and Tong 75 correlation for externally finned swirl tube

Name, geometry and transversal incident flux profile	Longitudinal incident flux profile	L_h (mm)	P_{local} (MPa)	T_{in} (°C)	T_{local} (°C)	$T_{sat}-T_{local}$ (°C)	G ($Mg.m^{-2}.s^{-1}$)	V_{axial} (m/s)	ΔP_{lineic} (MPa/m)	ICHF (MW/m^2)	Geom.WCHF (MW/m^2)	FE WCHF (MW/m^2)	FE peaking factor	Shot number
1996 JAERI OFHC-Cu OD = 10 mm ID = 7 mm PBEF Ion Beam Geom. peaking factor: 1.43	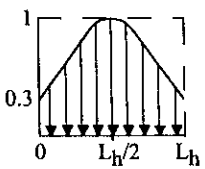	160	1.0	30	36	143	25.1	25	1.01	32.7	46.7	41.5	1.27	E59
		160	1.0	30	37	142	20.0	20	0.71	30.7	43.9	39.1	1.27	E54
		160	1.0	28	35	144	18.1	18	0.56	30.7	43.9	39.1	1.27	E47
		160	1.0	28	37	142	16.1	16	0.46	30.7	43.9	39.1	1.27	E38
		160	1.0	28	37	142	14.1	14	0.37	27.0	38.6	34.5	1.28	E44
		160	1.0	29	38	141	12.0	12	0.29	25.3	36.1	32.2	1.27	E41
		160	1.0	28	38	141	10.0	10	0.18	21.8	31.1	27.5	1.26	E23
		160	1.0	28	40	139	8.1	8	0.13	21.8	31.1	27.6	1.27	E29
		160	1.0	28	39	140	6.0	6	0.07	15.3	21.9	19.1	1.25	E30

Table 1: thermal hydraulic results for smooth tube

Name, geometry and transversal incident flux profile	Longitudinal incident flux profile	L_h (mm)	P_{local} (MPa)	T_{in} (°C)	T_{local} (°C)	$T_{sat}-T_{local}$ (°C)	G ($Mg.m^{-2}.s^{-1}$)	V_{axial} (m/s)	ΔP_{lineic} (MPa/m)	ICHF (MW/m^2)	Geom.WCHF (MW/m^2)	FE WCHF (MW/m^2)	FE peaking factor	Shot number
1996 JAERI Material :OFHC-Cu OD = 10 mm ID = 7 mm Twist ratio:3 Tape thickness:0.35 mm Tape material: Inconel 625 PBEF Ion Beam Geom. peaking factor: 1.43	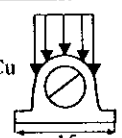 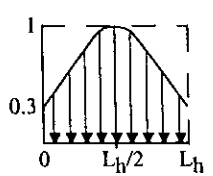	160	1.5	24	43	155	14.0	14	0.90	39.6	56.6	52.3	1.32	B52
		160	1.5	25	45	153	12.0	12	0.68	36.8	52.6	49.1	1.33	B47
		160	1.5	25	48	150	10.0	10	0.47	34.7	49.6	46.9	1.35	B30
		160	1.5	25	50	148	8.0	8	0.30	30.7	43.9	42.0	1.37	B36
		160	1.5	25	54	144	6.0	6	0.17	27.0	38.6	37.7	1.40	B39
		160	1.5	24	56	142	4.1	4	0.09	19.8	28.3	27.8	1.40	B42
		160	1.0	22	37	142	20.0	20	1.82	45.8	65.4	59.1	1.29	C35
		160	1.0	21	37	142	18.0	18	1.49	43.5	62.1	58.4	1.34	C30
		160	1.0	21	38	141	16.0	16	1.19	41.6	59.4	54.0	1.30	C25
		160	1.0	21	40	139	14.1	14	0.93	39.6	56.6	52.6	1.33	C20
		160	1.0	22	41	138	12.1	12	0.71	36.8	52.6	48.5	1.32	C15
		160	1.0	23	45	135	10.0	10	0.48	34.7	49.6	46.6	1.34	B57
		160	1.0	24	47	132	8.0	8	0.32	28.9	41.3	39.1	1.35	B60
		160	1.0	23	50	129	6.0	6	0.17	25.4	36.3	34.8	1.37	C05
		160	1.0	23	58	121	4.0	4	0.11	21.8	31.1	31.1	1.43	C10

Table 2: thermal hydraulic results for externally-finned swirl tube

Name, geometry and transversal incident flux profile	Longitudinal incident flux profile	L_h (mm)	P_{local} (MPa)	T_{in} (°C)	T_{local} (°C)	$T_{sat}-T_{local}$ (°C)	G ($Mg.m^{-2}.s^{-1}$)	V_{axial} (m/s)	ΔP_{linear} (MPa/m)	ICHF (MW/m^2)	Geom.WCHF (MW/m^2)	FE WCHF (MW/m^2)	FE peaking factor	Shot number
1996 **JAERI** Material : OFHC-Cu ISO 261 : B 0205 M7 OD = 10 mm ID = 7 mm ID_2 = 6.35 mm P = 1 mm ID_1 = 5.91 mm H = 0.87 mm 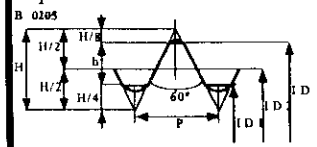 PBEF Ion Beam Geom. peaking factor:1.43	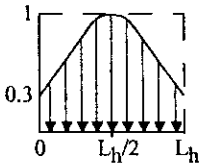 	160	1.5	28	48	150	10.0	10	0.46	32.7	46.7			E12
		160	1.5	28	51	147	8.0	8	0.31	30.7	43.9			E18
		160	1.0	30	43	136	19.9	20	2.00	41.6	59.4			E07
		160	1.0	31	44	135	17.9	18	1.60	41.6	59.4			E04
		160	1.0	29	44	135	15.9	16	1.26	39.6	56.6			D35
		160	1.0	30	46	133	13.9	14	0.96	36.8	52.6			D32
		160	1.0	31	47	132	11.9	12	0.70	32.7	46.7			D19
		160	1.0	31	49	130	10.0	10	0.46	30.7	43.9			D09
		160	1.0	31	51	128	8.0	8	0.32	27.0	38.6			D14
		160	1.0	31	54	125	6.0	6	0.15	23.7	33.9			D22
		160	1.0	30	65	114	4.0	4	0.06	23.7	31.1			D28
1996 **JAERI** Material : OFHC-Cu ISO 261 : B 0205 M12 OD = 15 mm ID = 12 mm ID_2 = 10.86 mm P = 1.75 mm ID_1 = 10.11 mm H = 1.51 mm PBEF Ion Beam Geom. peaking factor: 1.25	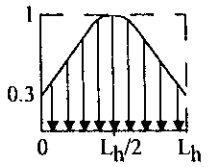 	160	1.0	25	32	147	15.0	15	0.81	32.7	40.9			B06
		160	1.0	26	33	146	14.0	14	0.68	32.7	40.9			B03
		160	1.0	26	42	137	12.0	12	0.52	30.7	38.4			A55
		160	1.0	26	35	144	10.0	10	0.36	28.9	36.1			A41
		160	1.0	25	35	144	8.0	8	0.24	27.0	33.8			A45
		160	1.0	25	37	142	6.0	6	0.16	23.7	29.7			A48
		160	1.0	25	42	141	4.0	4	0.09	16.8	21.0			A51
1996 **JAERI** Material : OFHC-Cu ISO 261 : B 0205 M16 OD = 19 mm ID = 16 mm ID_2 = 14.70 mm P = 2 mm ID_1 = 13.84 mm H = 1.73 mm PBEF Ion Beam Geom. peaking factor: 1.19	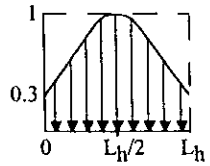 	160	1.0	25	32	147	8.0	8	0.23	27.0	32.1			B20
		160	1.0	30	38	141	6.0	6	0.13	23.7	28.1			B15
		160	1.0	30	40	139	4.0	4	0.04	18.3	21.7			B10
		160	1.0	25	32	147	2.0	2	0.001	6.8	8.0			B22

Table 3: thermal hydraulic results for screw tubes

Name, geometry and transversal incident flux profile	Longitudinal incident flux profile	L_h (mm)	P_{local} (MPa)	T_{in} (°C)	T_{local} (°C)	$T_{sat}-T_{local}$ (°C)	G ($Mg.m^{-2}.s^{-1}$)	V_{axial} (m/s)	ΔP_{lineic} (MPa/m)	ICHF (MW/m^2)	Geom.WCHF (MW/m^2)	FE WCHF (MW/m^2)	FE peaking factor	Shot number
1996 **JAERI** Material: OFHC-Cu Wall thickness: 2.5 mm Fin thickness: 3 mm Gap between fins: 3 mm 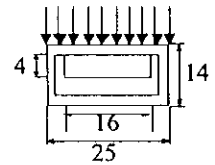 PBEF Ion Beam Geom. Peaking factor: 1.25	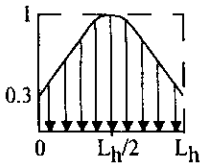 	160	1.0	26	30	149	10.0	10	0.80	25.3	31.6			Aa26
		160	1.0	31	41	138	8.0	8	0.48	23.7	29.6			A08
		160	1.0	28	35	144	8.0	8	0.49	23.7	29.6			Aa16
		160	1.0	31	44	135	5.9	6	0.33	22.0	27.5			A05
		160	1.0	28	38	141	6.0	6	0.29	22.0	27.5			Aa08
		160	1.0	31	48	131	4.0	4	0.18	19.8	24.8			A11
		160	1.0	27	42	137	4.0	4	0.11	19.8	24.8			Aa11
		160	1.0	30	42	137	2.0	2	0.07	6.8	8.5			A16
		160	1.0	27	36	143	2.0	2	0.004	6.8	8.5			Aa13
		160	0.7	26	36	129	8.5	9	0.53	23.7	29.6			A22
		160	0.7	26	38	127	6.0	6	0.32	23.7	29.6			A23
		160	0.7	26	44	121	4.0	4	0.18	19.8	24.8			A29

Table 4: thermal hydraulic results for hypervapotron